LncCCAT1 interaction protein PKM2 upregulates SREBP2 phosphorylation to promote osteosarcoma tumorigenesis by enhancing the Warburg effect and lipogenesis

FEIFEI PU[1*], JIANXIANG LIU[1*], DOUDOU JING[1*], FENGXIA CHEN[2], XIN HUANG[1], DEYAO SHI[1], WEI WU[1], HUI LIN[1], LEI ZHAO[1], ZHENHAO ZHANG[1], XIAO LV[1], BAICHUAN WANG[1], ZHICAI ZHANG[1] and ZENGWU SHAO[1]

[1]Department of Orthopedics, Union Hospital, Tongji Medical College, Huazhong University of Science and Technology, Wuhan, Hubei 430022; [2]Department of Radiation and Medical Oncology, Zhongnan Hospital, Wuhan University, Wuhan, Hubei 430071, P.R. China

Received October 19, 2021; Accepted December 30, 2021

DOI: 10.3892/ijo.2022.5334

Abstract. Pyruvate kinase M2 (PKM2) plays an important role in the consumption of glucose and the production of lactic acid, the striking feature of cancer metabolism. The association of PKM2 with osteosarcoma (OS) has been reported but its role in OS has yet to be elucidated. To study this, PKM2-bound RNAs in HeLa cells, a type of cancer cells widely used in the study of molecular function and mechanism, were obtained. Peak calling analysis revealed that PKM2 binds to long noncoding RNAs (lncRNAs), which are associated with cancer pathogenesis and development. Validation of the PKM2-lncRNA interaction in the human OS cell line revealed that lncRNA colon cancer associated transcript-1 (lncCCAT1) interacted with PKM2, which upregulated the phosphorylation of sterol regulatory element-binding protein 2 (SREBP2). These factors promoted the Warburg effect, lipogenesis, and OS cell growth. PKM2 appears to be a key regulator in OS by binding to lncCCAT1. This further extends the biological functions of PKM2 in tumorigenesis and makes it a novel potential therapeutic for OS.

Introduction

Osteosarcoma (OS) is the most common primary malignant bone tumor in children and adolescents, and it is characterized by malignant spindle stromal cells (1). Great progress has been made in the treatment of OS. Currently, the main treatment methods include surgical resection, neoadjuvant chemotherapy, radiotherapy, and immunotherapy, but the prognosis of patients has not significantly improved (2). According to the literature, the 5-year survival rate for patients with OS is between 37.5 and 77.6%; however, the average survival time of patients with recurrence or pulmonary metastasis is generally less than one year, and the 5-year survival rate is often less than 20% (3). Therefore, it is crucial to elucidate the molecular mechanisms underlying the occurrence and development of OS and to search for new molecular markers and therapeutic targets.

Long non-coding RNAs (lncRNAs) play an important role in OS and can significantly regulate pathophysiological processes and phenotypes, including gene expression, chromatin remodeling, and post-transcriptional regulation (4). LncRNAs can play an important role by targeting microRNAs (miRNAs or miRs), signaling pathways, cytokines, and genes (5). Previous studies by our group have shown that lncRNAs, as competitive endogenous RNAs or 'molecular baits' regulate the expression of miRNAs and are involved in the occurrence, development, and metastasis of OS (6,7). With the advancement of research, a variety of lncRNAs can be used as potential prognostic indicators, biomarkers, and therapeutic targets for OS (6,7). LncRNA AFAP1-AS1 is overexpressed in osteosarcoma and plays an oncogenic role in OS through the RhoC/ROCK1/p38MAPK/Twist1 signaling pathway, these findings indicated a novel molecular mechanism underlying the tumorigenesis and progression of OS. AFAP1-AS1 could serve as a promising therapeutic target in OS treatment (7).

Cancer cells use glycolysis for energy supply regardless of whether they are in an anoxic environment, which is also known as aerobic glycolysis or the Warburg effect (8). Pyruvate kinase M2 (PKM2) is a key enzyme involved in glycolysis (9). In recent years, studies have found that PKM2 is overexpressed in cancer tissues and, in addition to regulating metabolism, PKM2 can also enter the nucleus and participate in gene transcription regulation (10-12). The overexpression

Correspondence to: Dr Zengwu Shao or Dr Zhicai Zhang, Department of Orthopedics, Union Hospital, Tongji Medical College, Huazhong University of Science and Technology, 1277 Jiefang Avenue, Wuhan, Hubei 430022, P.R. China
E-mail: 1985XH0536@hust.edu.cn
E-mail: zhangzhicai@hust.edu.cn

[*]Contributed equally

Key words: lncRNA colon cancer associated transcript-1, pyruvate kinase M2, RNA binding protein, Warburg effect, osteosarcoma

of PKM2 predicts a poor prognosis for patients with OS, and PKM2 may serve as a novel target for treatment (13). Another study confirmed that metformin increased the sensitivity of OS stem cells to cisplatin by inhibiting the expression of PKM2 (14). The miR-1294/PKM2 signaling cascade plays important roles in the regulation of OS progression (15).

Through direct binding to specific sequence element(s), RNA binding proteins (RBPs) play a pivotal role in co- and post-transcriptional RNA regulatory events (16). Acquisition of a drug-resistant (DR) phenotype relies on the upregulation of the polypyrimidine tract binding protein 1 (PTBP1), which in turn is recruited to the pyruvate kinase pre-mRNA and favors splicing of the oncogenic PKM2 variant (17). Although the association between PKM2 and OS has been previously reported (18), the function and mechanism of PKM2 as an RBP in OS, have not been studied. The targeted regulation of PKM2 by multiple pathways to inhibit the proliferation, migration, and invasion of cancer cells and promote their apoptosis has become a new direction in the treatment of cancers (19).

To study the potential function of PKM2 in OS, PKM2-bound RNAs in HeLa cells were obtained. Peak calling analysis revealed that PKM2 binds to lncRNAs associated with cancer pathogenesis and development. The PKM2-lncRNA interaction in the human OS cell line was then validated, showing that the lncRNA colon cancer associated transcript-1 (lncCCAT1) regulated the proliferation of OS through PKM2 and promoted the Warburg effect. The specific mechanism of action was as follows: lncCCAT1 promoted the dephosphorylation of PKM2 in the nucleus by recruiting Cdc25A, which in turn promoted glycolysis. LncCCAT1 promoted fat synthesis in OS, and PKM2 phosphorylated sterol regulatory element-binding protein 2 (SREBP2) at T610 without impairing kinase activity. These findings support the hypothesis that PKM2 is a key regulatory gene in OS as an RBP. PKM2 could function in OS by binding to lncCCAT1, further extending the biological functions of PKM2 in tumorigenesis and thereby, making it a novel potential therapeutic for OS.

Materials and methods

Cell culture. All cell lines, including HeLa (cat. no. TCHu187), hFOB 1.19 (cat. no. GNHu14), HOS (cat. no. TCHu167), and U2OS (cat. no. SCSP-5030) were purchased from the Cell Bank of the Typical Culture Preservation Committee of the Chinese Academy of Sciences [National Center of Authenticated Cell Cultures (NCACC)]. KHOS-240S (cat. no. CRL-1545) was obtained from the American Type Culture Collection. These cells were routinely cultured in RPMI-1640 medium (HyClone; Cytiva) and supplemented with 10% (v/v) FBS (HyClone; Cytiva) and 1% penicillin-streptomycin (Gibco; Thermo Fisher Scientific, Inc.). All the cells were cultured in 5% CO_2 at 37˚C. Protein expression and reconstitution experiments were conducted using the established stable cell lines. All cell lines were routinely tested for mycoplasma infection and confirmed to be negative.

Plasmid overexpression. Primer pairs used for hot fusion were designed using CE Design V1.04 (Vazyme Biotech Co., Ltd.). Each primer comprised a fragment of a gene-specific sequence and a 17-30 bp sequence of the pIRES-hrGFP-1a vector (forward primer, agcccgggcggatccgaattcATGTCGAAG CCCCATAGTGAAG and reverse primer, gtcatccttgtagtcctc gagCGGCACAGGAACAACACGC). The pIRES-hrGFP-1a vector was digested with *Eco*RI and *Xho*I (New England BioLabs, Inc.) at 37˚C for ~2-3 h. The enzyme-digested vector was then run on a 1.0% agarose gel and purified using a QIAGEN GmbH column kit (cat. no. 12123; QIAGEN GmbH) according to the manufacturer's instructions. Total RNA was isolated from HeLa cells using TRIzol (cat. no. 15596-018; Invitrogen; Thermo Fisher Scientific, Inc.). Purified RNA was transcribed for cDNA using oligodT primers. The insert fragment was then synthesized by PCR amplification. A linearized vector digested by *Eco*RI and *Xho*I and the PCR insert were added to a PCR microtube for ligation with ClonExpress® II One Step Cloning Kit (Vazyme Biotech Co., Ltd.). Plasmids were introduced into the *Escherichia coli* strain (cat. no. EC11303; Sigma-Aldrich; Merck KGaA) by chemical transformation. A total of $5x10^5$ cells were plated onto LB agar plates containing 1 μl/ml ampicillin (cat. no. A6920; Beijing Solarbio Science & Technology Co., Ltd.), and incubated overnight at 37˚C. Colonies were screened by colony PCR (28 cycles) using universal primers (located on the backbone vector). The insert sequence was verified by Sanger sequencing. GAPDH was used as the control gene to assess the effects of PKM2 or SREBP2 overexpression via reverse transcription-quantitative PCR (RT-qPCR) and western blotting. Comparisons were performed using the paired Student's t-test using GraphPad Prism software v9.2.0 (GraphPad Software, Inc.).

Short hairpin RNA (shRNA) transfection. To stably knockdown lncCCAT1 or PKM2, specific shRNAs as well as corresponding controls (sh-NC) were synthesized by Sangon Biotech Co., Ltd. The shRNA sequences were then were subcloned into pSUPER vectors (OligoEngine) as previously described (20). For stable transfection, OS cells reaching 80% confluency were transfected with pSUPER plasmids containing indicated shRNAs (2.5 μg/ml) by the use of Lipofectamine 2000 (Invitrogen; Thermo Fisher Scientific, Inc.) at 25˚C for 15 min, followed by treatment with 600 μg/ml G418 (1 mg/ml; Stratagene; Agilent Technologies, Inc.) for 2 weeks. Thereafter, the stably transfected cells were selected from the remaining colonies. The selected cells were further kept for two weeks before following application. The transfection efficiency was verified using RT-qPCR. The sequences of shRNAs used are provided in Table SI.

Immunoprecipitation (IP). HeLa cells ($5x10^6$) were first lysed in ice-cold lysis buffer (1X PBS, 0.5% sodium deoxycholate, 0.1% SDS and 0.5% NP40) with RNase inhibitor (Takara Bio, Inc.) and a protease inhibitor (Beijing Solarbio Science & Technology Co., Ltd.) on ice for 5 min. The mixture was then vigorously vibrated and centrifuged at 13,000 x g at 4˚C for 20 min to remove cell debris. The supernatant was incubated with DynaBeads protein A/G (Thermo Fisher Scientific, Inc.) conjugated with anti-FLAG antibody (MDL no. MFCD02262912) or normal IgG (MDL no. MFCD00212351; both from Sigma Aldrich; Merck KGaA) at 4˚C overnight. The beads were washed with low-salt wash buffer, high-salt wash buffer, and 1X PNK buffer (product no. SAB4200134;

Sigma Aldrich; Merck KGaA). The beads were resuspended in elution buffer and then divided into two groups, one for RNA isolation from PKM2-RNA complexes and the other for the western blotting assay for PKM2.

Improved RNA immunoprecipitation sequencing (iRIP-seq) library preparation and sequencing. Cells were cross-linked on ice with UV irradiation type C (254 nm) at 400 mJ per cm^2 in the presence of cold PBS (4 ml per 15-cm dish). Cells were scraped off and pelleted at 1,000 x g at 4˚C and stored at -80˚C until further use. Cells lysis was performed in cold wash buffer (1X PBS, 0.1% SDS, 0.5% NP-40 and 0.5% sodium deoxycholate) supplemented with a 200 U/ml RNase inhibitor (Takara Biotechnology Co., Ltd.) and protease inhibitor cocktail (Roche Diagnostics) and incubated on ice for 30 min. The clear cells were lysed by centrifugation at 13,200 x g for 10 min at 4˚C followed by the addition of RQ I (1 U/μl; Promega Corporation) to a final concentration of 1 U/μl and incubation in a water bath for 3 min at 37˚C. A cooling reaction was subsequently performed for 5 min on ice before proceeding, and the reaction was terminated with the addition of EDTA. For immunoprecipitation, the supernatant was incubated overnight at 4˚C with 10 μg Flag-antibody and control IgG-antibody. The immunoprecipitation was further incubated with protein A/G Dynabeads for 2 h at 4˚C. After applying a magnet and removing the supernatants, the beads were sequentially washed with lysis buffer, high-salt buffer (250 mM Tris 7.4, 750 mM NaCl, 10 mM EDTA, 0.1% SDS, 0.5% NP-40 and 0.5 deoxycholate), and PNK buffer (50 mM Tris, 20 mM EGTA and 0.5% NP-40) two times, respectively. The beads were resuspended in Elution buffer (50 nM Tris 8.0, 10 mM EDTA and 1% SDS), and the suspension was incubated for 20 min in a heat block at 70˚C to release the immunoprecipitated RBP with crosslinked RNA and vortex. The magnetic beads were removed on the separator. The supernatant was transferred to a clean 1.5-ml microfuge tube. Proteinase K (Roche Diagnostics) was added into the 1% input (without immunoprecipitated) and immunoprecipitated RBP with crosslinked RNA, with a final concentration of 1.2 mg/ml and incubated for 120 min at 55˚C. The RNA was purified with TRIzol reagent. The Illumina ScriptSeq™ v2 RNA-Seq Library Preparation Kit (Epicentre; Illumina Inc.) was used for the cDNA libraries. The cDNAs were purified and amplified; PCR products corresponding to 200-500 bps were purified, quantified and stored at -80˚C until used for sequencing. PKM2-bound RNAs were isolated by IP of anti-FLAG using TRIzol. cDNA libraries were prepared with the KAPA RNA Hyper Prep Kit (kit code KK8541; KAPA Biosystems, Inc.; Roche Diagnostics) according to the manufacturer's protocol. The quality of samples was identified by FastQC v0.11.6 (http://www.bioinformatics.babraham.ac.uk/projects/fastqc/), and high-throughput sequencing of the cDNA libraries was performed on the Illumina X10 platform (Illumina, Inc.) for 150 bp paired-end sequencing. The series record GSE184327 (https://www.ncbi.nlm.nih.gov/geo/query/acc.cgi?acc=GSE184327) provides access to all of our data and is the accession no. that should be quoted in any manuscript referring to the data. For high-throughput sequencing, the libraries were prepared following the manufacturer's instructions and applied to an Illumina Nextseq500 system for 150 nt paired-end sequencing by ABlife (Wuhan), Inc.

RT-qPCR. Total RNA was isolated from the cells using the E.Z.N.A® Total RNA Kit I R6834 (Omega Bio-Tek, Inc.), and the RNA was measured using NanoDrop ND-1000 (Thermo Fisher Scientific, Inc.). Purified RNA was reverse-transcribed into cDNA (25˚C, 5 min; 42˚C, 1 h; and 70˚C, 5 min) using the HiScript III RT SuperMix (Vazyme Biotech Co., Ltd.). RT-qPCR (95˚C for 5 min and 30 cycles at 95˚C for 10 sec, 57˚C for 30 sec and 72˚C for 30 sec, and finally 72˚C for 10 min) was then performed using the Step One system (Applied Biosystems™; Thermo Fisher Scientific, Inc.) and AceQ Universal SYBR qPCR Master Mix (Vazyme Biotech Co., Ltd.). Gene expression was calculated using the $2^{-\Delta\Delta Cq}$ method (21) and normalized to the reference gene GAPDH. Primer sequences are presented in Table SI.

Data analysis of iRIP-seq. After reads were aligned onto the genome, only uniquely mapped reads were used for subsequent analysis. The ABLIRC strategy was used to identify the binding regions of PKM2 on the genome (22). Reads with an overlap of at least 1 bp were clustered as peaks. For each gene, a computational simulation was used to randomly generate reads with the same number and length as the reads in the peaks. The output reads were further mapped to the same genes to generate a random maximum peak height from the overlapping reads. The entire process was repeated 500 times. All the observed peaks with heights higher than those of the random max peaks ($P<0.05$) were selected. The IP and input samples were independently analyzed by the simulation, and the IP peaks that overlapped with the input peaks were removed. The target genes of IP were finally determined by the peaks, and the binding motifs of the IP protein were revealed using the HOMER software (http://bio.informatics.iupui.edu/homer). The fuzznuc software (EMBOSS; http://embossgui.sourceforge.net/demo/fuzznuc.html) was used to obtain the specific positions of the two motifs on lncRNANEAT1, lncRNAPVT1, and lncCCAT1 combined with the peak.

Functional enrichment analysis. To sort out functional categories of peak-associated genes (target genes), Gene Ontology (GO) terms and Kyoto Encyclopedia of Genes and Genomes (KEGG) pathways were identified using KOBAS 2.0 (http://kobas.cbi.pku.edu.cn) (23). The hypergeometric test and Benjamini-Hochberg false discovery rate control procedure were used to define the enrichment of each term.

Western blotting. The sample of cells was resuspended in 40 liters elution buffer [50 mM Tris-Cl (pH 8.0), 10 mM EDTA (pH 8.0), and 1% SDS], and incubated at 70˚C for 20 min with shaking (13,200 x g). The sample was then pulse-centrifuged at 13,200 x g and the supernatant was transferred to a new Eppendorf tube placed on a magnetic separator. The complexed samples were eluted after boiling in water with 1X SDS buffer for 10 min. The protein concentration was evaluated using BCA Pierce Protein Assay Kit (Pierce Biotechnology, Inc.; Thermo Fisher Scientific, Inc.). Subsequently, 20 μg of proteins was loaded and separated by 10% SDS-PAGE, followed by

transferring to polyvinylidene fluoride (PVDF) membranes (Roche Diagnostics). TBST buffer (20 mM Tris-buffered saline and 0.1% Tween-20) containing 5% non-fat milk powder was used for incubating the membranes for 1 h at room temperature. The membranes were then processed with primary antibodies for 1 h at room temperature, and then with HRP-conjugated secondary antibody (product code ab288151; 1:10,000; Abcam) at room temperature for 1 h. Finally, the bands were visualized using the enhanced chemiluminescence (ECL) reagent (EMD Millipore) and quantified via the ImageJ2X version 1.8.0 software (National Institutes of Health). The primary antibodies were as follow: PKM2 (product code ab85555; 1:500), hexokinase 2 (HK2; product code ab209847; 1:1,000), 6-phosphofructo-2-kinase/fructose-2,6-bisphosphatase-3 (PFKFB3; product code ab181861; 1:2,000), lactate dehydrogenase (LDHA; product code ab52488; 1:10,000); pyruvate dehydrogenase kinase 1 (PDK1; product code ab202468; 1:2,000; all from Abcam), p-PKM2^{S37} (cat. no. 11456; 1:1,000; Signalway Antibody LLC), Cdc25A (cat. no. 21145; 1:1,000; Signalway Antibody LLC), acetyl-coenzyme A carboxylase 1 (ACC1; product code ab45174; 1:2,000; Abcam), ATP citrate lyase (ACLY; product code ab40793; 1:10,000; Abcam), fatty acyl-CoA elongase 6 (ELOVL6; cat. no. 24672; 1:500; Signalway Antibody LLC), fatty acid synthase (FASN; product code ab128870; 1:10,000; Abcam), stearoyl-CoA desaturase 1 (SCD1; product no. 2794; 1:1,000; Cell Signaling Technology, Inc.), stearoyl-CoA desaturase 5 (SCD5; cat. no. 27911; 1:2,000; Signalway Antibody LLC), SREBP2 (product code ab30682; 1:1,000), α-Actinin (product code ab68194; 1:1,000), and Histone-H3 (product code ab1791, 1:5,000; all from Abcam).

Fluorescence in situ hybridization (FISH) analysis. HOS and U2OS cells grown on slides were washed with PBS and fixed with 4% paraformaldehyde for 10 min at 72˚C. Following treatment with the protease reagent, the slides were incubated with pre-hybridization buffer at 40˚C for 4 h, and then hybridized overnight with a digoxin-labeled probe at 40˚C. After washing by PBS, the slides were incubated with a HRP-conjugated anti-digoxin antibody (cat. no. NEF832001EA; PerkinElmer, Inc.). The slides were then incubated with SABC-FITC at 37˚C for 30 min after washing, followed by processing with 0.2 μmol/l 4',6-diamidino-2-phenylindole (cat. no. D9542; Sigma Aldrich; Merck KGaA) containing antifade mounting solution. The images were obtained under a fluorescence microscope (Leica, SP8 laser confocal microscope). The lncCCAT1 FISH probe sequence is presented in Table SI.

Cell viability assay. Cell viability was measured using Cell Counting Kit-8 (CCK-8) (Sigma Aldrich; Merck KGaA) in accordance with the manufacturer's instructions. According to the experimental grouping design, 2,000 HOS and U2OS cells were seeded in each of the 96 wells of the plates overnight at 37˚C, and then further cultured for 0, 24 48, or 72 h. CCK-8 solution (10 μl; Dojindo Molecular Technologies, Inc.) was then added, and the absorbance at 450 nm was measured using a SpectraMax microtitration plate reader (Molecular Devices, LLC).

5-Ethynyl-20-deoxyuridine (EdU) assay. EdU staining was performed according to the instructions of the EdU kit (Guangzhou RiboBio Co., Ltd.). In short, 4x10^3 HOS and U2OS cells were cultured in DMEM containing EdU for 2 h at 37˚C. The cells were fixed in 4% formaldehyde for 30 min. After staining with DAPI for 10 min at 37˚C, EdU-positive cells were observed and counted under a fluorescence microscope (Nikon Corporation).

Colony formation assay. A total of 800 HOS and U2OS cells were seeded into 12-well plates and incubated at 37˚C for 2 weeks. OS cells were fixed with 4% paraformaldehyde at 37˚C for 60 min and stained with 2% crystal violet at 37˚C for 20 min. Colonies with >50 cells were counted. Images were obtained using a camera (Nikon Corporation).

Glucose uptake assay. The glucose uptake capacity of HOS and U2OS cells was measured using a glucose assay kit (cat. no. N13195; Thermo Fisher Scientific, Inc.) according to the manufacturer's instructions. First, cells were seeded in 96-well plates (5x10^4 cells/well) and cultured in DMEM without glucose. The cells were then rinsed with PBS and incubated with 2-NBDG at 37˚C for 30 min. When the cells were rewashed with HBSS, the fluorescence intensity of the cells was detected.

Lactate content measurement. The L-Lactate Assay Kit (cat. no. 700510; Cayman Chemical Company) was used to assess both the intracellular and extracellular lactate content of HOS and U2OS cells. OS cells (5x10^4) were first cultured at 4˚C in DMEM basic medium containing 10% FBS and then in DMEM basic medium containing 0.5% FBS for 4 h. After collecting the cells, the lactate content was measured according to the manufacturer's instructions.

Extracellular acidification rate (ECAR) and oxygen consumption rate (OCR) analyses. According to the manufacturer instructions (Seahorse Bioscience, Inc.; Agilent Technologies, Inc.), the ECAR and OCR of HOS and U2OS cells were measured in a 96-well plate (5x10^4 cells/well) using Seahorse XF Analyzers. One day prior to the experiment, the cells were placed on cell culture microplates. When ECAR was measured, 10 mM glucose, 1 μM oligomycin, and 100 mM 2-deoxyglucose were added first. When OCR was detected, 1 μM oligomycin, 1 μM FCCP, and 1 μM rotenone were added to the microplates. The ECAR and OCR values were calculated according to methods reported in the literature (24).

NADPH/NADP$^+$ assay. According to the experimental methods reported in the literature (25), HOS and U2OS cells (1x10^5 cells/well) were cultured in 6-well plates for 48 h and then in glucose-free medium. The cells were extracted with an extraction buffer, and the supernatant containing NADPH/NADP$^+$ was extracted after centrifugation (10,000 x g at 37˚C for 10 min). The supernatant was heated at 60˚C for 30 min to decompose NADP$^+$, then cooled on ice, and quickly spun to remove the sediment. Part of the supernatant was reacted with NADP$^+$ circulation buffer and enzyme mixture for 5 min at room temperature to convert NADP$^+$ to NADPH. OS cells were analyzed using the NADPH assay kit (product code ab65349; Abcam) according to the manufacturer's instructions and the NADP$^+$/NADPH quantification kit (cat. no. S0179;

Beyotime Institute of Biotechnology) according to the manufacturer's instructions.

NAD^+ assay. Complex I, also known as NADH dehydrogenase, catalyzes the dehydrogenation of NADH to NAD^+. The activity of this enzyme was calculated by measuring the oxidation rate of NADH at 340 nm. According to the operation method reported in the literature (26), NAD^+ was detected using the Micro Mitochondrial Respiratory Chain Complex I Activity Assay Kit (cat. no. BC0515; Beijing Solarbio Science & Technology Co., Ltd.) according to the manufacturer's instructions.

Glutathione (GSH) measurement. GSH levels were determined using the GSH-Glo™ assay (cat. no. V6912, Promega Corporation). Fluorescein derivatives were converted to fluorescein in the presence of GSH. According to the manufacturer's instructions, the cells were incubated with 2.1 mM GSH-Glo™ reagent for 30 min at 25˚C. Luminescence was detected using a BioTek Synergy H1 Hybrid plate reader (BioTek Instruments, Inc.).

ATP measurement. HOS and U2OS cells were inoculated onto 96-well plates at ~8,000 cells/well, after interference with lncCCAT1, following the manufacturer's instructions to carry out the experiment (ATPlite; PerkinElmer, Inc.). The BMG (Thermo Fisher Scientific, Inc.) reader was used to screen all the plates to obtain the luminescence signal, and the ATP concentration was normalized to the protein concentration.

Glucose 6-phosphate production analysis. HOS and U2OS cells were incubated with L-arginine (cat. no. A0013; Beijing Solarbio Science & Technology Co., Ltd.) and glucose-free F-12K (cat. no. 21127022, Gibco; Thermo Fisher Scientific, Inc.) medium for 30 min at 37˚C and then incubated with 7 mM L-glucose (cat. no. 20829; Cayman Chemical Company), 1 mM L-arginine, or 1 mM D-arginine (cat. no. A769515; Toronto Research Chemicals) for another 30 min at 37˚C. Cell lysates were then collected and glucose 6-phosphate content was determined using a Glucose-6-Phosphate Fluorometric Assay kit (cat. no. 700750-96 wells; Cayman Chemical Company). Finally, the concentration of glucose 6-phosphate in cells was determined according to the methods reported in the literature (27).

3-Phosphoglycerate (3-PG) production analysis. The production of 3-PG was determined according to the methods reported in the literature (28). The reaction buffer consisted of 200 mM HEPES, 100 mM KCl, 5 mM Na_2HPO_4, 0.5 mM EDTA, and 5 mM $MgCl_2$ at pH 7.4. Subsequently, 50 μl supernatant, 2 mM ATP, 0.1 mM NADH, 1 U/ml PGK, and 1 U/ml GAPDH were added to the reaction buffer.

RIP assay. According to the literature (29), the association between lncCCAT1 and PKM2 was determined using the Magna RIP RBP IP kit (cat. no. 17-700; Millipore; Merck KGaA) according to the manufacturer's instructions. PKM2 antibodies (cat. no. 11456; 1:1,000; Signalway Antibody LLC) were used for the RIP assay at 4˚C overnight with gentle rotation and co-precipitated RNA was used for cDNA synthesis and evaluated by RT-qPCR.

RNA pulldown assay. A DNA fragment containing the full-length lncCCAT1 sequence or a negative control sequence was PCR-amplified using T7 RNA polymerase (cat. no. 10881767001; Roche Diagnostics). The lncCCAT1 was labeled with biotin and the biotinylated RNA was incubated with cell lysate overnight. Then, streptavidin magnetic beads (cat. no. 072001; IPHASE) were added and incubated for 48 h at 37˚C. The products were treated with RNase-free DNase I (Roche Diagnostics) and purified with an RNeasy Mini Kit (cat. no. DXT-74134, Qiagen, Inc.), with the resulting RNA used for RT-qPCR assays.

Co-IP. Co-IP was performed as reported previously (29), and western blotting analysis was performed on input samples and IP samples. Co-IP verified the effect of lncCCAT1 on the interaction between Cdc25A and PKM2 using PhosphoSitePlus (https://www.phosphosite.org/homeAction) and NetPhos-3.1 (https://services.healthtech.dtu.dk/service.php?NetPhos-3.1). To further demonstrate that PKM2 acted as a phosphokinase at T610 of SREBP2, PKM2 in the cell line 293T (cat. no. SCSP-502; NCACC) was overexpressed. The phosphorylation of PKM2 at T610 of SREBP2 was demonstrated by adding the 0.5 mM PKM2 phosphorylation substrate phosphoenolpyruvate (PEP; product code ab34793; Abcam) at 30˚C for 3 h.

GST pulldown assay. The codon-optimized sequence of PKM2 was cloned into the expression GEX-4T-1 vector (*Eco*RI/*Xho*I, GE Healthcare; Cytiva). Approximately 100 μg of GST and GST-PKM2 fusion protein were immobilized in 50 μl of GSH agarose and equilibrated before incubation at 4˚C for 1 h to capture the GST fusion proteins. Then, 1 μg GST-core fusion protein was added and incubated at 4˚C overnight. After washing with a cracking buffer solution (cat. no. P001; Caisson Labs, Inc.) four times at room temperature for 5 min, the proteins were eluted in Laemmli buffer and analyzed by 10% SDS-PAGE at 95˚C for 15 min (cat. no. S1051-100; Beijing Solarbio Science & Technology Co., Ltd.).

IP coupled with western blotting (IP-WB). According to a previous study (30), OS cells were lysed with RIPA lysis buffer, and then proteins were diluted with NET-gelatin buffer. Subsequently, the samples were incubated with antibodies. After incubation with agarose-A/G (cat. no. sc-2001; Santa Cruz Biotechnology, Inc.) on a 40˚C shaker overnight, the precipitates were collected and washed. After adding 2X loading buffer, thermal denaturation was performed, and the proteins were separated by 10% SDS-PAGE at 95˚C for 15 min.

Lipid synthesis assay. OS cells were inoculated in 12-well plates ($5x10^4$ cells/well) following the methods reported in the literature (31). After 24 h, the cells were placed in FBS-free medium containing glucose and glutamine, and then incubated with ^{14}C-glucose for 2 h at 37˚C. After washing OS cells with PBS, lipids were extracted with hexane/isopropanol at room temperature. Finally, the lipids were dissolved

in chloroform and determined using a scintillation counter (Beckman Coulter, Inc.).

Cholesterol synthesis assay. As previously reported in the literature (32), OS cells were cultured in 6-well plates ($1x10^5$ cells/well), then LPDS, β-methylcyclodextrin, and $^{13}C_2$-sodium acetate were added and cultured for 24 h at 37˚C. The cells were washed with ice-cold PBS followed by 0.9% NaCl, and ice-cold methanol was added. The cells were collected, centrifuged, and methanol was added. The analysis was performed using an ultra-high-pressure liquid chromatography system (Thermo Fisher Scientific, Inc.).

Ethical approval. The procedures were approved (approval no. S2019009) by the Ethics Committee for Laboratory Animals of Huazhong University of Science and Technology (Wuhan, China). The animals were handled in strict compliance with the Guiding Principles for the Care and Use of Animals of the American Physiological Society (33).

Tumor xenografts. The *in vivo* study was approved by the Ethics Committee for Laboratory Animals of Huazhong University of Science and Technology (Wuhan, China). In brief, $5x10^6$ HOS cells transfected with sh-lncCCAT1 or sh-NC (control) were suspended in 200 μl PBS and injected subcutaneously into the backs of 8-week-old BALB/C nude female mice (mean weight, 23 g; Laboratory Animal Center, Huazhong University of Science and Technology, Wuhan, China). A total 6 mice (n=3/group) were involved in this experiment. No animals succumbed during this experiment. Each mouse was housed in a separate cage in a specific pathogen-free (SPF) laboratory (temperature, 28˚C; humidity, 50%; light/dark cycle, 10/14 h cycle), with free access to food and water. Animal health and behavior were monitored 3 times a week. The tumor size was measured with a caliper at 7, 10, 14, 17, 21, 24 and 28 days after inoculation (while the corresponding curves were drawn from the results tested at 7, 14, 21 and 28 days), and the volume was determined according to the formula of length x width^2 x 1/2. When the tumor volume reached 1,000 mm^3, the mice were euthanized via cervical dislocation. Mice were considered sacrificed when they had no response to stimulation via tweezers. Subsequently, the tumors were collected and weighed.

Immunohistochemical (IHC) analysis. IHC was performed as described in the literature (34). Tumors obtained from *in vivo* assays were paraffin-embedded and cut into 4-μm thick slices, followed by transferring to glass slides. After deparaffinization and hydration, the slides were placed in citrate buffer (pH 6.0) and heated in a microwave oven (high fire mode, 5 min) to retrieve antigen. Following cooling at 25˚C and endogenous peroxidase removal via 3% H_2O_2 (10 min), sections were stained overnight at 4˚C with HK-2 (product code ab209847; 1:500; Abcam;), LDHA (product code ab52488; 1:2,000; Abcam), FASN (product code ab128870; 1:450; Abcam), and SCD1 (cat. no. 2794S; 1:400; Cell Signaling Technology, Inc.). After processing with HRP-conjugated secondary antibody (product code ab97080; 1:2,000; Abcam) at 4˚C overnight, the sections were rinsed three times using TBST with 0.1% Tween-20 for 5 min, visualized via 3,3-diaminobenzidine (DAB) for 5 min at room temperature, and counterstained using hematoxylin for 1 min at room temperature. Scans were performed using an Aperio scanoscope (Leica Biosystems) and analyzed using the Aperio Imagescope software v6.0 (Leica Biosystems).

Statistical analyses. Three independent experiments were performed, and data from three repeated experiments were presented as the mean ± standard deviation (SD) and analyzed using IBM SPSS Statistics 22.0 (IBM Corp.). Student's t-test was used for the comparison between two groups. For comparisons between three or more groups, one-way ANOVA was performed followed by Dunnett's or Tukey's multiple comparison test. For comparison between two or more variables, two-way ANOVA was applied. $P<0.05$ was considered to indicate a statistically significant difference.

Results

iRIP-seq of PKM2 exhibits its binding preference on RNAs. As revealed in Fig. S1A and B, RT-qPCR and western blotting verified PKM2 overexpression in HeLa cells, a most popular cancer cell model widely used in the study of molecular function and mechanism. Western blotting results revealed successful IP of PKM2 in HeLa cells (Fig. S1C). The hierarchically clustered Pearson correlation matrix was obtained by comparing the transcript expression values for the input and PKM2 IP samples (Fig. S1D). The scatter plot of read abundance across the reference genome in paired samples showed an enriched preference for PKM2 IP samples (Fig. S1E). The enriched reads were distributed across the reference genome (Fig. S1F).

Peak analysis reveals the RNA binding features of PKM2. The peak distribution across the reference genome is presented in Fig. S2A, and the Venn diagram revealed the overlapped peaks in two replicate iRIP-seq samples (Fig. S2B). The HOMER software was used for motif analysis of the top ten preferred bound motifs of PKM2 (Fig. S2C). The top ten enriched GO biological processes and KEGG pathways of the PKM2-bound genes are presented in Fig. S2D.

PKM2 specifically binds to several lncRNAs. The peak sequence of bound lncRNAs in the overlap peak was used, and then HOMER was used to identify motifs on these sequences. After the motif comparison of the two results, it was determined that the two motifs AGAGAGA and UGGGU appeared relatively consistent, and thus the fuzznuc software was used to obtain the specific positions of the two motifs on lncRNANEAT1, lncRNAPVT1, and lncCCAT1 combined with the peak. The number of mRNAs, lncRNAs, small RNAS (sRNAs), and other types of RNAs bound by PKM2 in our iRIP-seq data were also obtained (Fig. 1A). The enriched abundance of RNAs bound by PKM2 in the IP sample and three PKM2-bound lncRNAs (PVT1, CCAT1, and NEAT1) are highlighted (Fig. 1B). Motif presentation revealed motif searching results for PKM2-bound lncRNAs and three specific PKM2-bound lncRNAs (Fig. 1C). The read density plot revealed the binding density distribution and motif regions of these three lncRNAs (Fig. 1D).

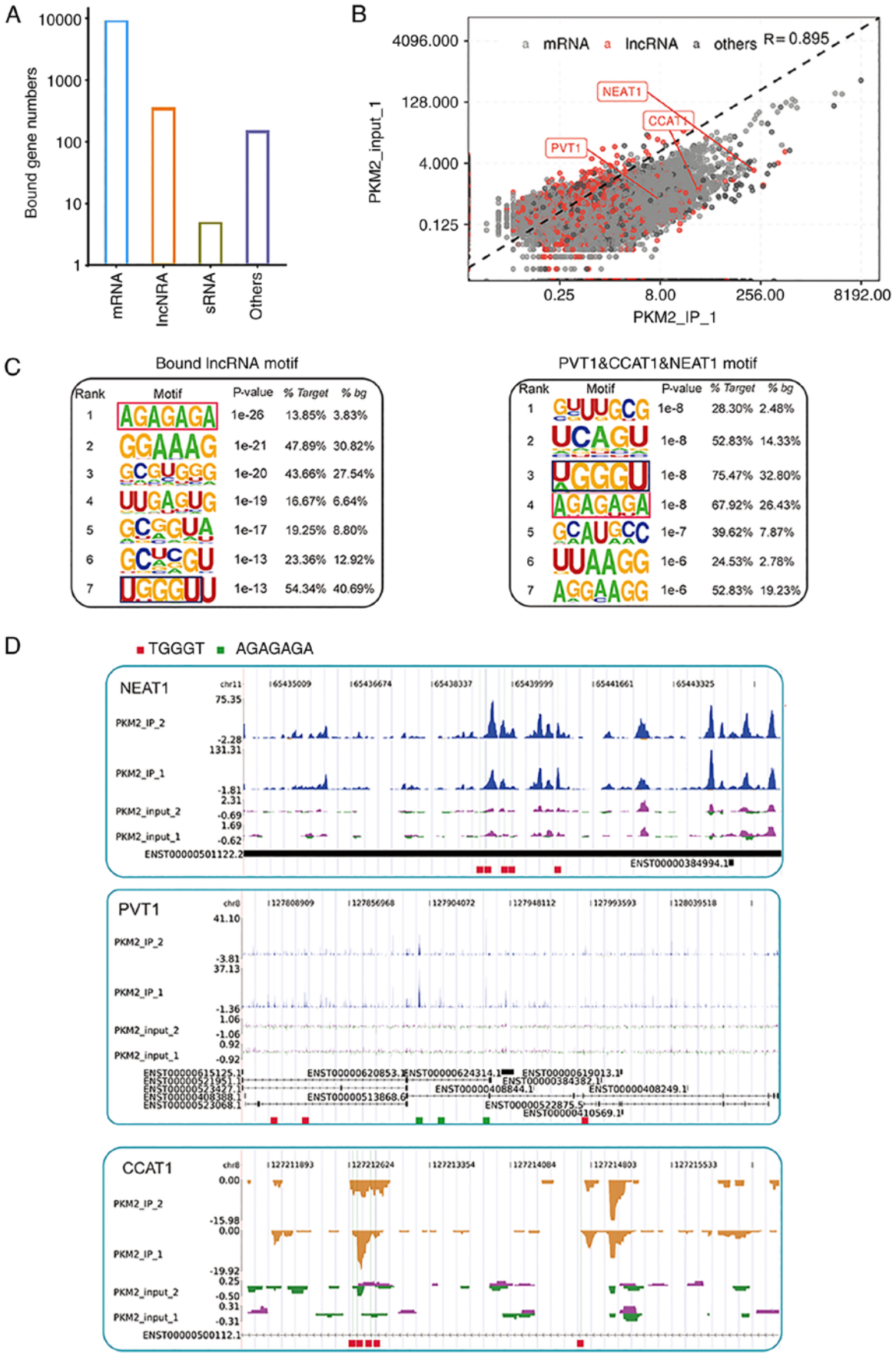

Figure 1. PKM2 specifically binds to several lncRNAs. (A) The number of mRNAs, lncRNAs, sRNAs, and other types of RNAs bound by PKM2 in iRIP-seq data. (B) The enriched abundance of RNAs bound by PKM2 in the IP sample and three PKM2-bound lncRNAs (PVT1, CCAT1, and NEAT1) are highlighted. (C) Motif presentation revealed motif searching results for PKM2-bound lncRNAs and three specific PKM2-bound lncRNAs. (D) The read density plot showed the binding density distribution and motif regions of these three lncRNAs. PMK2, pyruvate kinase M2; lncRNAs, long non-coding RNAs; iRIP-seq, improved RNA immunoprecipitation sequencing; IP, immunoprecipitation; sh-, short hairpin; NC, negative control.

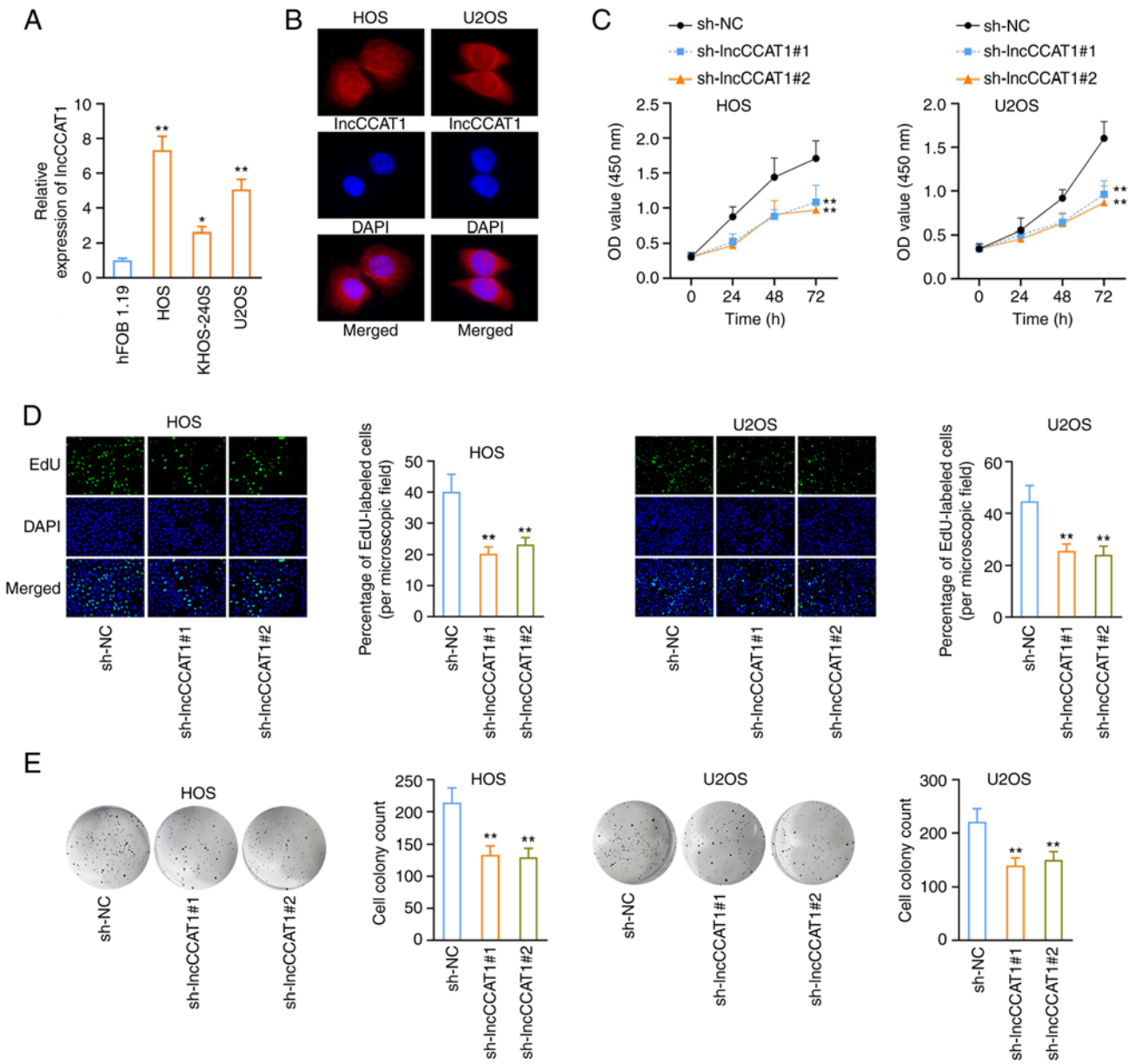

Figure 2. LncCCAT1 promotes the proliferation of OS cells. (A) LncCCAT1 was highly expressed in OS cells, particularly in the HOS and U2OS cell lines. (B) LncCCAT1 was distributed in both the nucleus and cytoplasm as determined in the FISH assay. (C and D) After interference with lncCCAT1, CCK-8 assay revealed that the proliferation of OS cells was reduced, and the number of positive cells was decreased as determined by EdU assay. (E) The clonal formation assay revealed that interference with lncCCAT1 reduced the number of OS cell clones. *P<0.05 and **P<0.01 vs. hFOB1.19 or sh-NC. lncCCAT1, lncRNA colon cancer associated transcript-1; OS, osteosarcoma; FISH, fluorescence *in situ* hybridization; CCK-8, Cell Counting Kit-8; EdU, 5-ethynyl-20-deoxyuridine; sh-, short hairpin; NC, negative control.

LncCCAT1 promotes the proliferation of OS cells. RT-qPCR was used to detect the expression of lncCCAT1 in human normal osteoblasts (HFOB 1.19) and OS cells (HOS, KHOS-240S, and U2OS). The results revealed that lncCCAT1 was highly expressed in OS cells, especially in the HOS and U2OS cell lines, for which subsequent experiments were conducted (Fig. 2A). The distribution of lncCCAT1 in HOS and U2OS cells after FISH was detected by fluorescence microscopy, and the results showed that lncCCAT1 was distributed in both the nucleus and cytoplasm (Fig. 2B), consistent with a previous study (35). The lncCCAT1 interference vector was constructed, and the interference groups with the optimal interference effect were selected for subsequent experiments (Fig. S3A). The CCK-8 assay revealed that the proliferation of HOS and U2OS cells was reduced after interference with lncCCAT1 (Fig. 2C), and the decreased number of positive cells in OS cells was detected by EdU (Fig. 2D). The clonal formation assay revealed that interference with lncCCAT1 reduced the number of OS cell clones (Fig. 2E).

LncCCAT1 promotes the Warburg effect in OS cells. Following interference with lncCCAT1, the amounts of glucose and lactic acid in the culture medium of HOS and U2OS cells were decreased (Fig. 3A and B). After detecting interference with lncCCAT1 with Seahorse XF Extracellular Flux Analyzers, the ECAR of HOS and U2OS cells was decreased (Figs. 3C and S4A), the OCR was increased (Figs. 3D and S4B), and the relative glycolysis rate (ECAR/OCR) was decreased

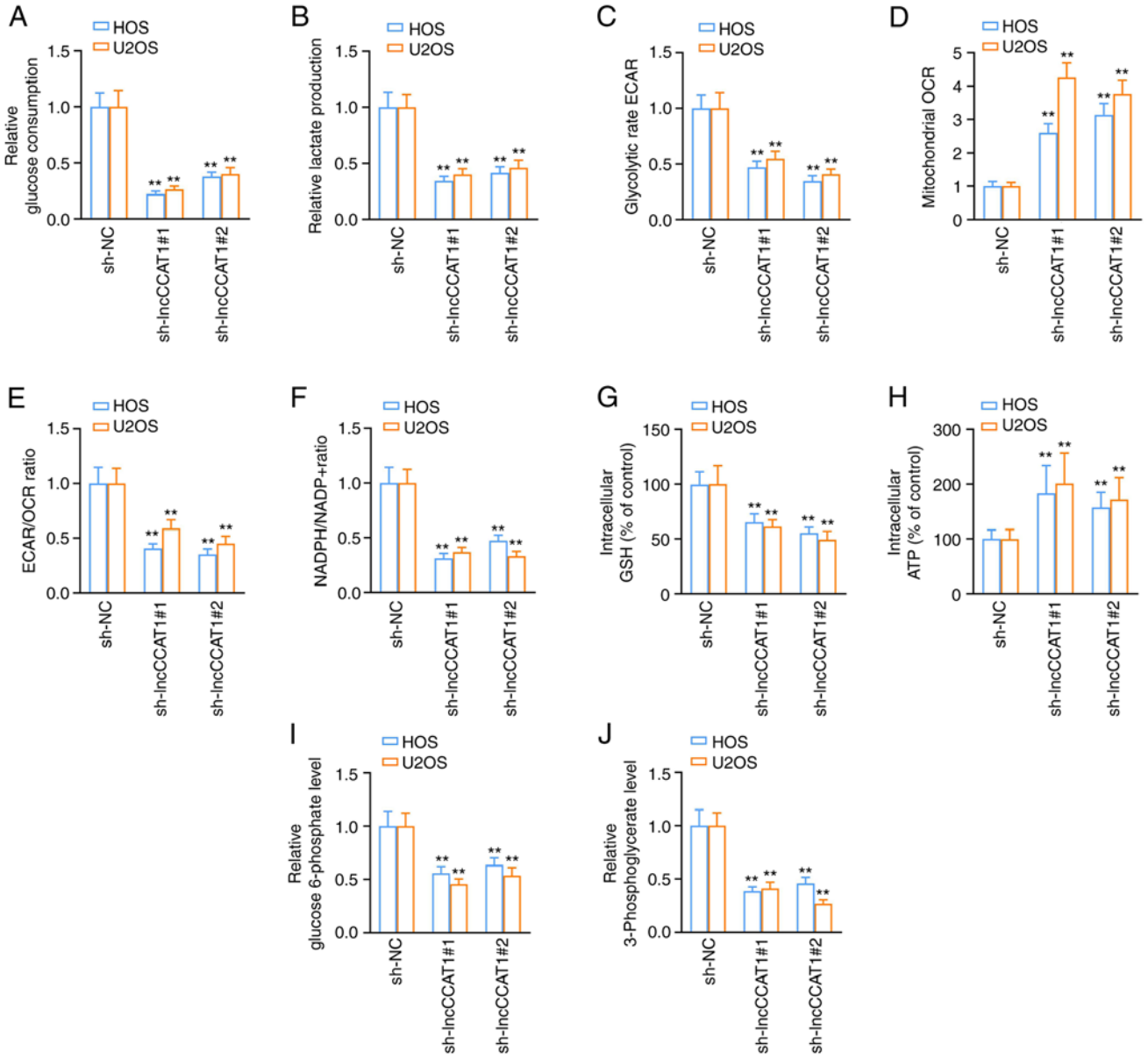

Figure 3. LncCCAT1 promotes the Warburg effect in OS cells. (A and B) Following interference with lncCCAT1, the amounts of glucose and lactic acid in the culture medium of HOS and U2OS cells was decreased. (C) After detecting interference with lncCCAT1 using Seahorse XF Extracellular Flux Analyzers, the ECAR of OS cells was decreased, (D) the OCR was increased, (E) the ECAR/OCR was decreased, (F) the level of NAPDH/NAPD+ was decreased, and (G) the intracellular GSH levels were decreased. After interference with lncCCAT1, (H) the levels of ATP, (I) glucose 6-phosphate, and (J) 3-phosphoglycerate in OS cells were decreased. **P<0.01 vs. sh-NC. lncCCAT1, lncRNA colon cancer associated transcript-1; OS, osteosarcoma; ECAR, extracellular acidification rate; OCR, oxygen consumption rate; GSH, glutathione; sh-, short hairpin; NC, negative control.

(Fig. 3E). The results of the NAPDH/NAPD$^+$ assay revealed that the level of NAPDH/NAPD$^+$ in OS cells decreased after interference with lncCCAT1 (Figs. 3F and S4C). The GSH GSH-Glo^{TM} assay revealed that intracellular GSH levels decreased after interference with lncCCAT1 (Fig. 3G). Following interference with lncCCAT1, the levels of ATP (Fig. 3H) were increased, and the levels of glucose 6-phosphate (Fig. 3I), and 3-PG (Fig. 3J) in HOS and U2OS cells were decreased.

LncCCAT1 promotes the proliferation of OS cells through PKM2. First, the binding effect of lncCCAT1 and PKM2 was verified. LncCCAT1 was enriched in PKM2 precipitation in HOS and U2OS cells, and the binding effect of lncCCAT1 and PKM2 was verified by the RIP assay (Fig. S5A). The binding effect of lncCCAT1 and PKM2 was verified by the RNA pulldown assay, and the results showed that lncCCAT1 could pulldown PKM2 (Fig. S5B). To investigate the regulation of lncCCAT1 on OS cell proliferation through PKM2, an interference vector of PKM2 (Fig. S3B) and an overexpression vector of lncCCAT1 were constructed (Fig. S3C) which were used in a rescue experiment. Overexpression of lncCCAT1 promoted the proliferation of OS cells, and after the interference with PKM2, reduced proliferation of OS cells as detected by CCK-8 (Fig. S5C), a reduced number of positive cells in OS cells as detected by EdU (Fig. S5D), and decreased OS cell clones as detected by the clonal formation assay (Fig. S5E) were revealed.

LncCCAT1 promotes the Warburg effect of OS cells through PKM2. The glucose assay kit was used to detect the glucose content in the culture medium of HOS and U2OS cells under different treatment conditions, and the results revealed that after overexpression of lnCCCAT1, the glucose content in cells increased; then, after interference with PKM2, glucose (Fig. S6A) and lactic acid (Fig. S6B) in the cells decreased. After overexpression of lncCCAT1, the Seahorse XF Extracellular Flux Analyzer detected that the ECAR was increased (Fig. S6C), the OCR was decreased (Fig. S6D), and therefore the ECAR/OCR was increased (Fig. S6E). On this basis, PKM2 was disrupted, and it was revealed that ECAR was decreased (Fig. S6C), the OCR was increased (Fig. S6D), and therefore the ECAR/OCR was decreased (Fig. S6E). Following overexpression of lncCCAT1, intracellular levels of NAPDH/NAPD$^+$ (Fig. S6F) and GSH (Fig. S6G) were increased, the intracellular levels of ATP were decreased (Fig. S6H), and the intracellular levels of glucose 6-phosphate (Fig. S6I) and 3-PG were increased (Fig. S6J). Following the aforementioned treatment, PKM2 was disrupted again, and the results revealed that the intracellular levels of NAPDH/NAPD$^+$ (Fig. S6F and K) and GSH (Fig. S6G) were decreased, the intracellular levels of ATP were increased (Fig. S6H), and the intracellular levels of glucose 6-phosphate (Fig. S6I) and 3-PG were decreased (Fig. S6J).

LncCCAT1 recruits Cdc25A to promote PKM2 dephosphorylation in the nucleus. The effect of lncCCAT1 on PKM2 nuclear localization in HOS and U2OS cells was observed by fluorescence microscopy. The results revealed that lncCCAT1 promoted the expression of PKM2 in the nucleus, however this expression was decreased after the interference of lncCCAT1 (Fig. 4A). Western blotting results revealed that the expression of PKM2 in the nucleus decreased after interference with lncCCAT1 (Fig. 4B), and studies have shown that nuclear PKM2 promotes the transcriptional activity of the myelocytomatosis oncogene (MYC) and thus, promotes glycolysis (36,37). Therefore, the transcriptional activity of MYC was examined. The transcription activity kit detected a decrease in MYC transcription activity after interference with lncCCAT1 (Fig. 4C), and the expression of the MYC-related genes were reduced (Fig. 4D). These results indicated that lncCCAT1 promoted the expression of PKM2 in the nucleus, activated the transcription activity of MYC, and promoted glycolysis.

Next, how lncCCAT1 regulates PKM2 nuclear translocation was explored. In HOS and U2OS cells, western blotting detected the expression of PKM2 and p-PKM2 after interference with lncCCAT1. The results revealed that lncCCAT1 could inhibit the phosphorylation of serine 37 in PKM2, suggesting that lncCCAT1 could recruit some phosphatases to act on PKM2 (Fig. 4E). Phosphatase Cdc25A has been reported to act on PKM2 in the nucleus (38). In HOS and U2OS cells, lncCCAT1 in the nucleus and cytoplasm were biotinized by RNA pulldown, and Cdc25A expression was detected by western blotting. The results showed that lncCCAT1 in the nucleus could be pulled down to Cdc25A after biotinization (Fig. 4F). Following the RIP assay, RT-qPCR was used to detect the expression of lncCCAT1, and the results confirmed that lncCCAT1 could recruit Cdc25A (Fig. 4G). Co-IP verified the effect of lncCCAT1 on the interaction between Cdc25A and PKM2, and the results revealed that lncCCAT1 promoted the interaction between Cdc25A and PKM2 when lncCCAT1 interfered (Fig. 4H). The aforementioned experimental results demonstrated that lncCCAT1 promoted the dephosphorylation of PKM2 in the nucleus by recruiting Cdc25A, thus promoting glycolysis.

In order to further explore whether PKM2 as an RBP of lncCCAT1, could play a role in lncCCAT1, it has been reported that RBP can stabilize RNA structure and lncCCAT1 plays a role in linking transcriptional complexes in the nucleus (39,40). Therefore, it was hypothesized that PKM2 could stabilize the structure of lncCCAT1. Following PKM2 interference, HOS and U2OS cells were treated with α-amanitin, and the expression levels of lncCCAT1 and GAPDH in the nucleus were detected by RT-qPCR. The results showed that PKM2 could stabilize lncCCAT1 (Fig. S7).

Phosphorylation of PKM2 at T610 of SREBP2. In HOS cells, the interaction protein of PKM2 was screened by GST pulldown combined mass spectrometry, and SREBP2 was revealed to interact with PKM2 (Fig. 5A). The Co-IP experiment also confirmed the interaction between SREBP2 and PKM2 (Fig. 5B). To predict the phosphorylation sites of SREBP2 on which PKM2 could act, an overexpression vector (pcDNA3.1) that inserted different fragments of SREBP2 was constructed; then, the GST pulldown assay was used to analyze the fragments that could bind to PKM2. Different overexpression vectors with GST tags were inserted into HOS cells, and the results of the GST pulldown experiment indicated that PKM2 may act on the phosphorylation sites of SREBP2 between 600 and 630 (Fig. 5C). A Co-IP assay was used to detect the effect of lncCCAT1 on the interaction between PKM2 and SREBP2, and the results revealed that interfering lncCCAT1 did not affect the interaction between PKM2 and SREBP2 (Fig. S8A). The PhosphoSitePlus and NetPhos-3.1 were used to predict the phosphorylation sites of SREBP2, and the two most likely phosphorylation sites in the range of 600-630 were T610 and S627 (Fig. S8B).

A stable cell line, HOS-SREBP2, overexpressing SREBP2 (Fig. S3D) was successfully constructed. In HOS-SREBP2 cells, IP-WB detected the effect of interference with PKM2 on the phosphorylation of SREBP2 in the nucleus; results showed that PKM2 affected phosphorylation at threonine (T) but not at serine. Therefore, the phosphorylation site of PKM2 on SREBP2 was identified as T610, and the molecular weight of SREBP2 protein was 123.72 kDa (Fig. 5D). A stable cell line HOS-SREBP2^{T610M} overexpressing the threonine mutant at site 610 of SREBP2 was constructed (Fig. S3E). In HOS-SREBP2 (wild-type, WT) and HOS-SREBP2^{T610M} (T610M) cells, the total protein content of SREBP2 was not affected by the T610 site, and the phosphorylation of SREBP2 T610 greatly affected protein expression in the nucleus (Fig. 5E). Further studies revealed that PKM2-mediated phosphorylation of T610 did not affect the protein synthesis of SREBP2 (Fig. 5F). Therefore, it was hypothesized that T610 affects the protein ubiquitination degradation process of SREBP2, rather than the synthesis process. IP-WB detected the ubiquitination of SREBP2 in the nucleus after PKM2 interference, indicating that PKM2-mediated phosphorylation of SREBP2 at T610 affected the stability of SREBP2 (Fig. 5G).

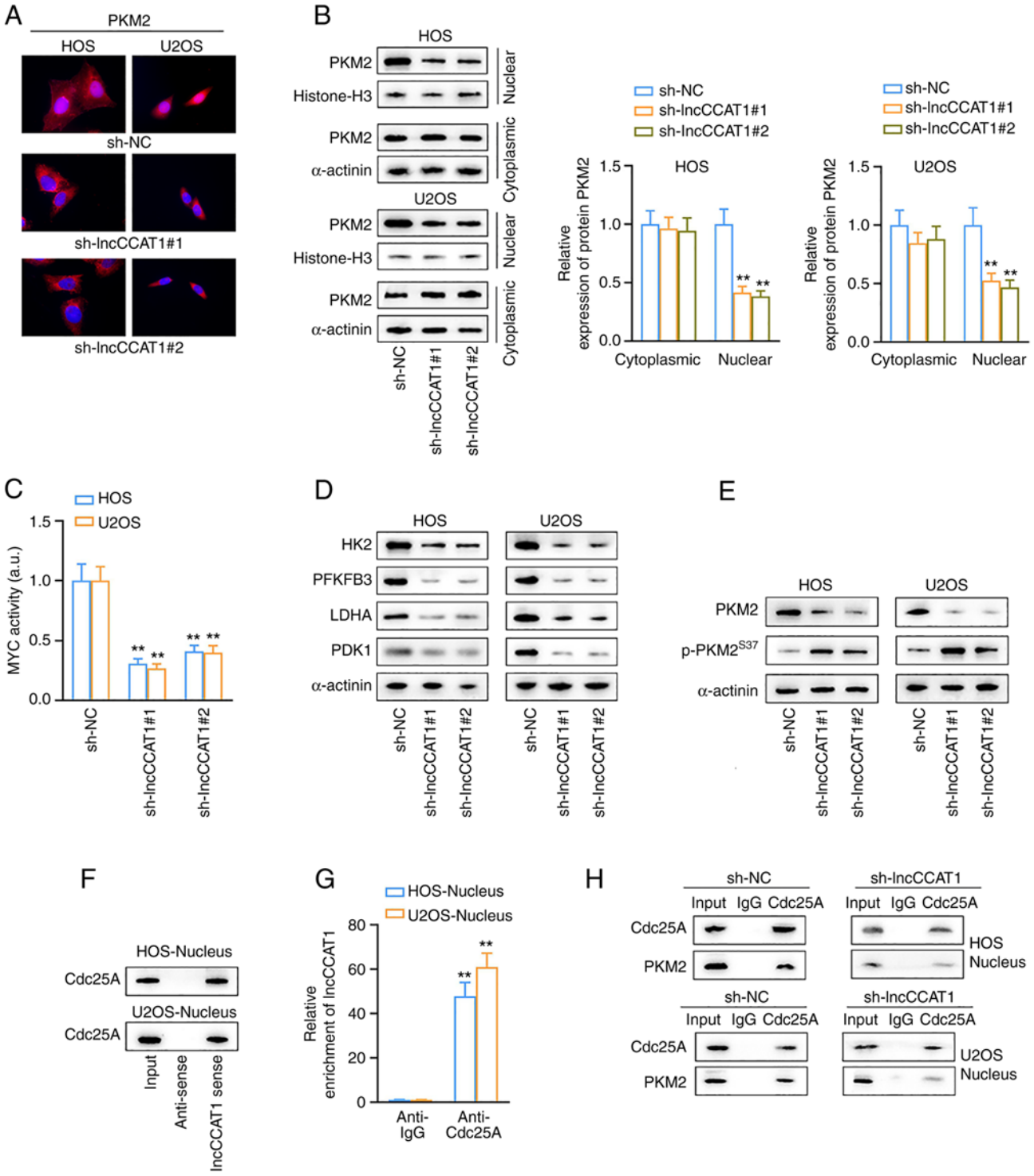

Figure 4. LncCCAT1 promotes the Warburg effect in OS cells. (A) The effect of lncCCAT1 on PKM2 nuclear localization in HOS and U2OS cells was observed by fluorescence microscopy. (B) Western blotting results showed that the expression of PKM2 in the nucleus decreased after interference with lncCCAT1. (C and D) The transcription activity kit detected a decrease in MYC transcription activity after interference with lncCCAT1, and the expression of the MYC-related genes were reduced. (E) LncCCAT1 inhibited the phosphorylation of serine 37 in PKM2. (F) LncCCAT1 in the nucleus could be pulled down to Cdc25A after biotinization. (G) After the RIP assay, RT-qPCR detected the expression of lncCCAT1, and lncCCAT1 could recruit Cdc25A. (H) Co-IP verified that lncCCAT1 promoted the interaction between Cdc25A and PKM2 when lncCCAT1 interfered. **P<0.01 vs. sh-NC. lncCCAT1, lncRNA colon cancer associated transcript-1; OS, osteosarcoma; PMK2, pyruvate kinase M2; MYC, myelocytomatosis oncogene; RIP, RNA immunoprecipitation; RT-qPCR, reverse transcription-quantitative PCR; sh-, short hairpin; NC, negative control.

In 293T-PKM2 cells, the phosphorylation of SREBP2 serine site was detected after the GST pulldown assay. The results revealed that PKM2 could phosphorylate T620 of SREBP2 only in the presence of PEP (Fig. 5H). It has been reported that phosphorylation of PKM2 at lysine (K) 367 plays a decisive role in PKM2 phosphokinase activity (41). Therefore, the mutant vector PKM2^{K367} was transferred into 293T cells to purify the PKM2-K^{367M}

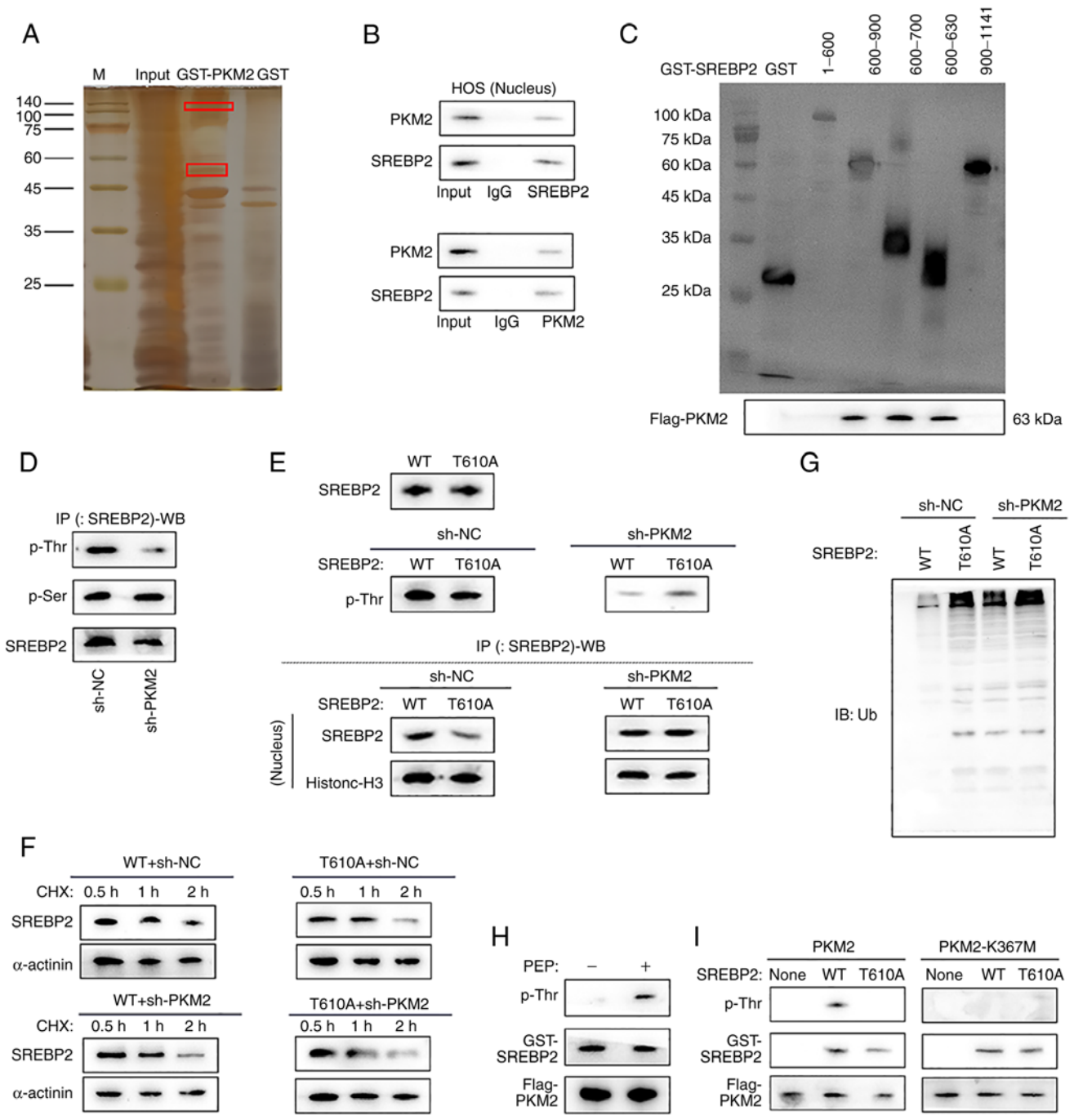

Figure 5. Phosphorylation of PKM2 at T610 of SREBP2. (A) SREBP2 was found to interact with PKM2 screened by GST pulldown combined mass spectrometry. (B) The Co-IP experiment confirmed the interaction between SREBP2 and PKM2. (C) GST pulldown experiment indicated that PKM2 may act on the phosphorylation sites of SREBP2 between 600 and 630. (D) The phosphorylation site of PKM2 on SREBP2 was identified as T610, and the molecular weight of SREBP2 protein was 123.72 kDa. (E) In HOS-SREBP2 (wild-type, WT) and HOS-SREBP2^{T610M} (T610M) cells, the total protein content of SREBP2 was not affected by the T610 site, and the phosphorylation of SREBP2 T610 greatly affected protein expression in the nucleus. (F) PKM2-mediated phosphorylation of T610 did not affect the protein synthesis of SREBP2. (G) IP-WB detected the ubiquitination of SREBP2 in the nucleus after PKM2 interference, and PKM2-mediated phosphorylation of SREBP2 at T610 affected the stability of SREBP2. (H) The phosphorylation of SREBP2 serine site was detected after the GST pulldown test, and PKM2 could phosphorylate T620 of SREBP2 only in the presence of PEP. (I) GST pulldown assay detected PKM2 could phosphorylate SREBP2 at T610. PMK2, pyruvate kinase M2; SREBP2, sterol regulatory element-binding protein 2; IP-WB, IP coupled with western blotting; sh-, short hairpin; NC, negative control.

protein, and a GST pulldown test was performed to verify the interaction between PKM2 and SREBP2 *in vitro*. In HOS-SREBP2 (WT) and HOS-SREBP2^{T610M} (T610M) cell culture media, and after exogenously adding PKM2 or PKM2-K367M, phosphorylation of SREBP2 was detected after GST pulldown assay. The results revealed that when kinase activity was not impaired, PKM2 could phosphorylate SREBP2 at T610 (Fig. 5I).

LncCCAT1 promotes lipogenesis in OS cells. In HOS and U2OS cells, the expression of several key genes that regulate lipogenesis were detected after interference with lncCCAT1.

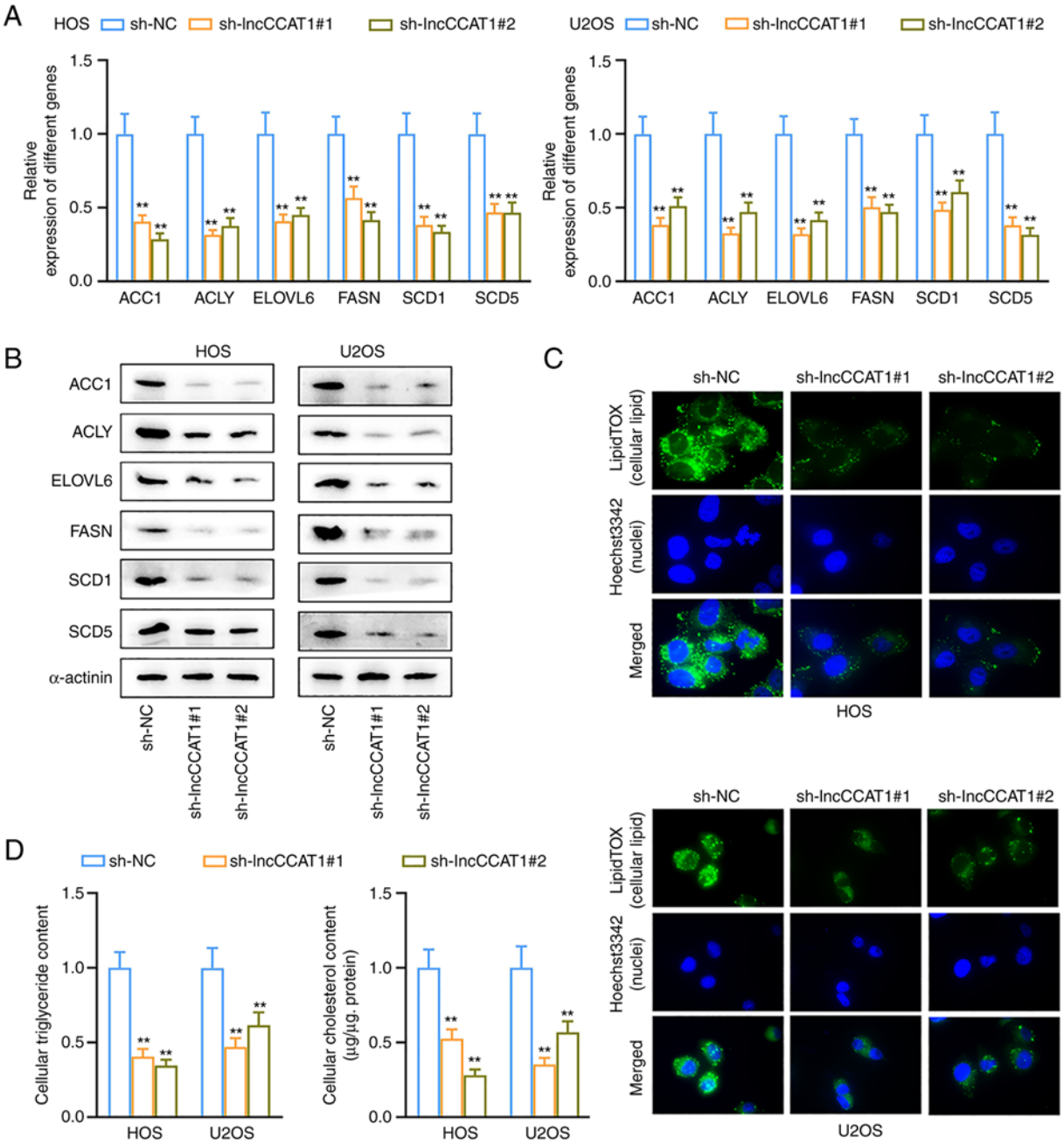

Figure 6. LncCCAT1 promotes lipogenesis in OS cells. (A and B) RT-qPCR and western blotting revealed that the expression of key genes in lipogenesis decreased after interference with lncCCAT1. (C) Fluorescence microscopy revealed that interference with lnCCCAT1 reduced the lipid content of OS cells. (D) In HOS and U2OS cells, the triglyceride and cholesterol contents decreased after interference with lncCCAT1. **P<0.01 vs. sh-NC. lncCCAT1, lncRNA colon cancer associated transcript-1; OS, osteosarcoma; RT-qPCR, reverse transcription-quantitative PCR; sh-, short hairpin; NC, negative control.

The RT-qPCR and western blotting results showed that the expression of key genes in lipogenesis decreased after interference with lncCCAT1 (Fig. 6A and B). Fluorescence microscopy revealed that interference with lnCCCAT1 reduced the lipid content of OS cells (Fig. 6C). In HOS and U2OS cells, the triglyceride and cholesterol contents decreased after interference with lncCCAT1 (Fig. 6D). These results indicated that lncCCAT1 promoted lipogenesis in OS cells.

LncCCAT1 promotes tumor growth, the Warburg effect, and lipogenesis in vivo. In vivo results revealed that HOS cells interfered with lncCCAT1, which resulted in slower growth of xenografts (Fig. 7A) and lighter weight xenografts (Fig. 7B). The expression of glycolysis-related proteins in the two groups was detected by IHC, and the results revealed that the positive rates of HK2 and LDHA were decreased in the sh-lncCCAT1 group (Fig. 7C). Western blotting revealed that the expression levels of HK2, PFKFB3, LDHA, and PDK1 were decreased in the sh-lncCCAT1 group (Fig. 7D). The expression of the lipid synthesis-related proteins, FASN and SCD1, was detected by IHC, and the results revealed that the positive rates of FASN and SCD1 were decreased in the transplanted tumor of the sh-lncCCAT1 group (Fig. 7E). Western blotting revealed that the expression levels of ACC1, ACLY, ELOVL6, and SCD5 were decreased in the sh-lncCCAT1 group (Fig. 7F).

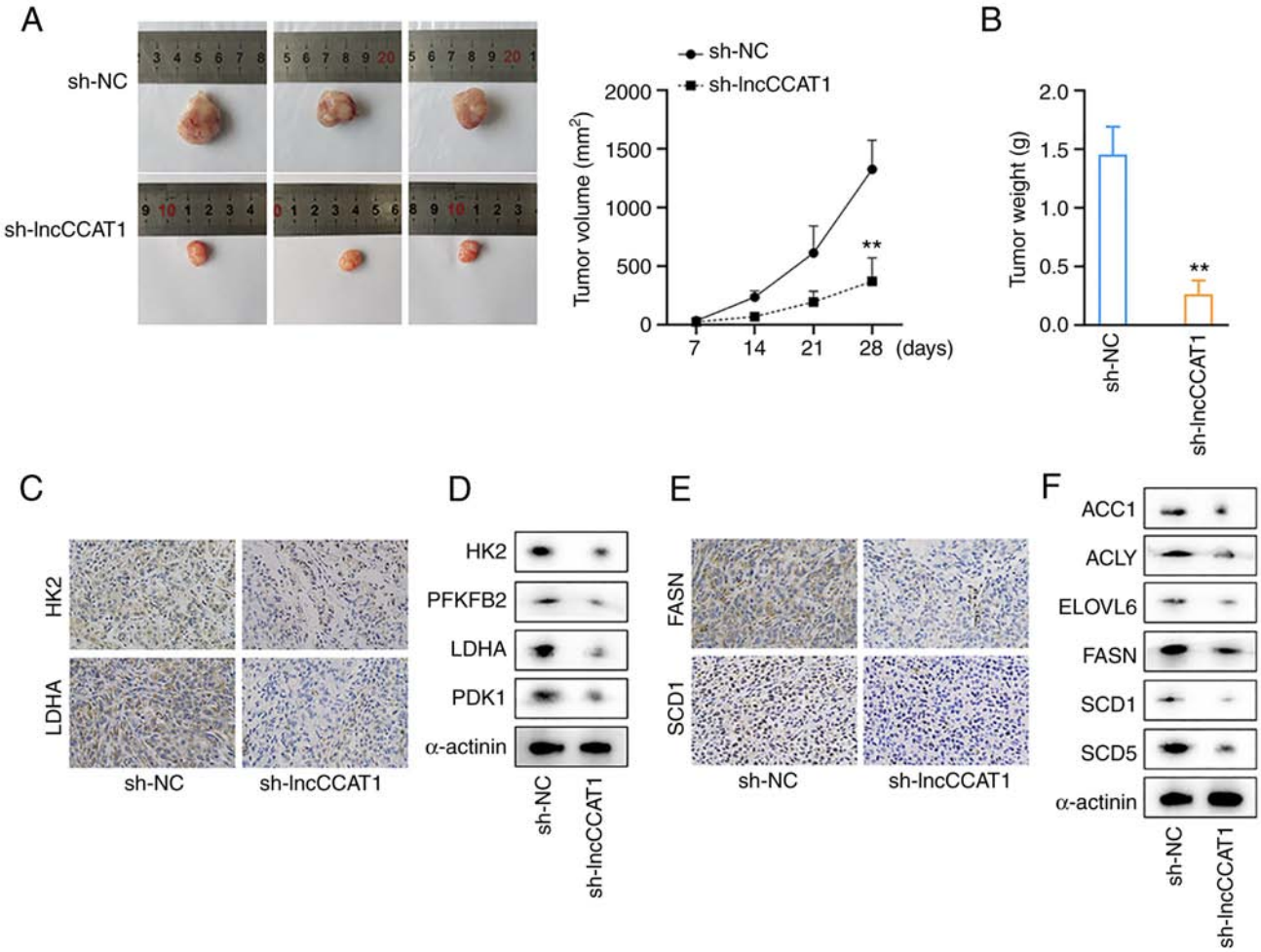

Figure 7. LncCCAT1 promotes tumor growth, the Warburg effect, and lipogenesis *in vivo*. (A and B) *In vivo* results revealed that HOS cells interfered with lncCCAT1, which resulted in slower growth of xenografts and lighter weight xenografts. (C) IHC detected the expression of glycolysis-related proteins, and the positive rates of HK2 and LDHA were decreased in the sh-lncCCAT1 group. (D) Western blotting showed that the expression levels of HK2, PFKFB3, LDHA, and PDK1 were decreased in the sh-lncCCAT1 group. (E) IHC detected the expression of FASN and SCD1, and the positive rates of FASN and SCD1 were decreased in the transplanted tumor of the sh-lncCCAT1 group. (F) Western blotting detected the expression of ACC1, ACLY, ELOVL6, and SCD5, and these proteins expression levels were decreased in the sh-lncCCAT1 group. $^{**}P<0.01$. lncCCAT1, lncRNA colon cancer associated transcript-1; IHC, immunohistochemistry; HK2, hexokinase; LDHA, lactate dehydrogenase; PFKFB3, 6-phosphofructo-2-kinase/fructose-2,6-bisphosphatase-3; PDK1, pyruvate dehydrogenase kinase 1; FASN, fatty acid synthase; SCD1, stearoyl-CoA desaturase 1; ACC1, acetyl-coenzyme A carboxylase 1; ACLY, ATP citrate lyase; ELOVL6, fatty acyl-CoA elongase 6; SCD5, stearoyl-CoA desaturase 5; sh-, short hairpin; NC, negative control.

Discussion

Previous studies have shown that PKM2 is correlated with the Enneking stage and distant metastasis in OS, and it has been identified as an independent prognostic factor for lethal disease (13-15,18,42). These studies revealed that PKM2 may represent a new therapeutic target for OS. In recent years, cancer metabolism has attracted increasing attention, and targeting cancer metabolism may be a promising strategy in cancer treatment (43). It is widely accepted that aerobic glycolysis provides the energy and phosphorus metabolites that tumor cells need to proliferate. As a glycolytic enzyme, PKM2 plays an important role in tumor glucose metabolism and cancer progression (44). Genetic alteration and epigenetic modification of PKM2 lead to dysregulation of tumor-associated genes, which finally results in tumor progression (45). Previous studies have reported that PKM2 can be translocated into the nucleus of tumor cells via a variety of mechanisms, which subsequently interact with the molecules responsible for cell proliferation, invasion, and metastasis (15,18,46).

At present, a variety of functional RNAs have been discovered, including mRNA for transmitting genetic information, transfer RNA (tRNA) and rRNA responsible for protein translation, small nuclear RNA (snRNA), microRNA, and non-coding RNA (ncRNA, including lncRNA and circular RNA) with special regulatory functions (47). Therefore, the function of RNA has gone far beyond its role as a mediator of genetic information transmission, and the binding of RNA to target molecules is a key step in the process of RNA function. The analysis and identification of RNA-protein interactions is key for exploring the function of RNA. Studying interacting RNA molecules in terms of proteins is a common approach, using RIP, cross-linking and immunoprecipitation (CLIP), and various derivative technologies (such as HiTS-CLIP, PAR-CLIP, iCLIP, and eCLIP) (48). iRIP-seq is a new technology to study RBPs, which adds UV-crosslinking and micrococcal nuclease (MNase) digestion in Clip-seq

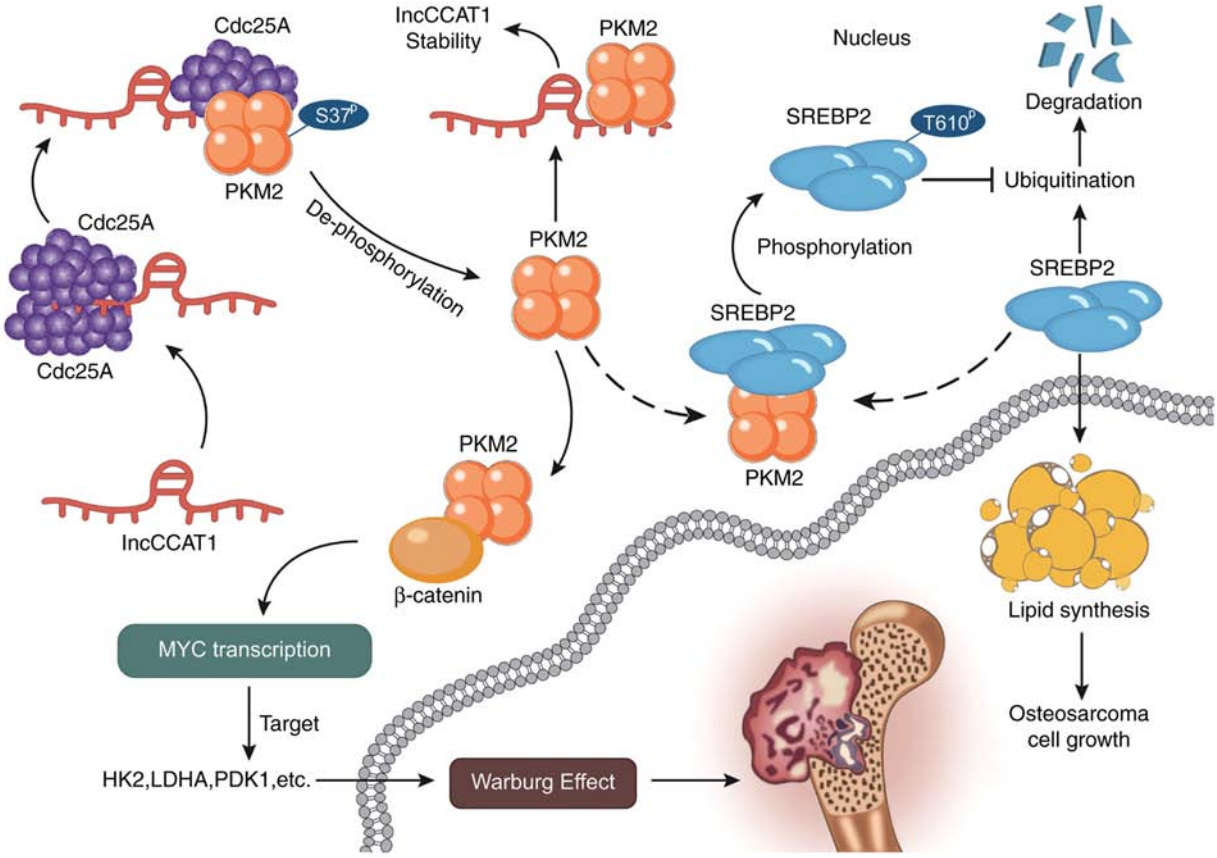

Figure 8. LncCCAT1 interaction protein PKM2 upregulates SREBP2 phosphorylation to promote osteosarcoma tumorigenesis by enhancing the Warburg effect and lipogenesis. lncCCAT1, lncRNA colon cancer associated transcript-1; PMK2, pyruvate kinase M2; SREBP2, sterol regulatory element-binding protein 2.

technology to the traditional RIP technology, and peaks and motif information combined with RBP are obtained by Clip-seq data analysis (49). iRIP-seq can not only accurately obtain the binding sites of RNA and protein in Clip-seq, but also retains the simplicity of RIP-seq (50).

LncRNAs are generally more than 200 bp in length and lack significant open reading frames, and thus they do not encode proteins (51). Although lncRNAs do not have the function of translating into proteins, they are widely involved in physiological and pathological activities of the human body, and mediate the occurrence and development of tumors (52). Studies have shown that lncRNAs play an important role in a variety of biological processes, can directly or indirectly interfere with gene expression in a variety of cancers, and regulate glucose metabolism in cancer cells (4,5,53). The most direct way to regulate glucose metabolism is to regulate the expression or activity of enzymes or kinases that affect its metabolism, and some signal transduction pathways also play an important role in glucose metabolism (54,55). The PKM2 target gene is not only lncCCAT1, but also other RNA and protein molecules. However, the interaction between lncCCAT1 and PKM2 revealed the regulatory function of PKM2. LncRNA HULC can directly bind to LDHA and PKM2, enhance interactions with the intracellular domain of the upstream kinase FGFR1, elevate phosphorylation, and modulate enzymatic activities. The elevation of LDHA activity and decrease in PKM2 activity both contribute to higher levels of glycolysis, thereby promoting cell proliferation (56).

A previous study has confirmed that peroxisome proliferator-activated receptor (PPAR) supports the transcription of PKM2 and can promote the occurrence of fatty liver (57). Lipid metabolism disorders play a key role in foam cell formation, and SREBP-1a regulates lipid synthesis through transcriptional activation of lipid genes. The interaction of PKM2 with nuclear SREBP-1a can enhance the phosphorylation of T106, further promoting the stabilization of SREBP-1a, and then increase the transcription of lipogenic genes such as FASN (58). In the present study, the expression of several key genes regulating lipogenesis was detected after interference with lncCCAT1, suggesting that lncCCAT1 could promote lipogenesis in OS. Therefore, in the occurrence and development of OS, it is theorized that in addition to the Warburg effect of PKM2, lipid metabolism also plays an important role.

To study the potential function of PKM2 in OS, PKM2-bound RNAs in HeLa cells were obtained. Peak calling analysis revealed that PKM2 binds to lncRNAs associated with cancer pathogenesis and development. Motif presentation revealed motif searching results for PKM2-bound lncRNAs and three specific PKM2-bound lncRNAs. The PKM2-lncRNA interaction in the human OS cell line was then validated, showing that the lncCCAT1 interaction protein PKM2 can promote OS tumorigenesis by enhancing the Warburg effect and lipid synthesis. SREBPs are a class of transcription factors

that regulate lipid homeostasis via modulating the expression of enzymes required for lipogenesis (59). SREBP2 has been demonstrated to modulate cholesterol synthesis and lipogenesis (60,61). The specific regulatory mechanism may be that lncCCAT1 promotes the dephosphorylation of PKM2 in the nucleus by recruiting Cdc25A, and phosphorylates SREBP2 at T610 to activate MYC transcriptional activity, thereby promoting glycolysis (Fig. 8). A study revealed that PKM2 is a novel substrate of Cdc25A, which plays an instrumental role in the Warburg effect. Cdc25A dephosphorylates PKM2 at S37 and promotes PKM2-dependent β-catenin transactivation, and c-MYC upregulated expression of the glycolytic genes PKM2, LDHA and GLUT1 (38).

These findings support the hypothesis that PKM2 is a key regulatory gene in OS as an RBP. PKM2 could function in OS by binding to lncCCAT1, further extending the biological functions of PKM2 in tumorigenesis, thus making it a novel potential therapeutic for OS.

Acknowledgements

The authors would like to thank Dr Y. Zhang (Center for Genome Analysis, ABLife Inc., Wuhan, China) for providing us with professional technology of iRIP-seq, and Dr J. Chen (Nanjing Nansi Biological Technology Co., Ltd., Nanjing, China) for the technical support for CoIP.

Funding

The present study was supported by The National Natural Science Foundation of China (grant no. 81904231) and the China Postdoctoral Science Foundation (grant no. 2020M672369).

Availability of data and materials

The authors declare that all the data supporting the findings in this study are available in this study and its Supplementary materials, or are available from the corresponding author on reasonable request.

Authors' contributions

FP, JL, DJ, ZhiZ and ZS designed the present study. FP, JL, DJ, FC, XH, DS, WW, HL, ZL, ZheZ, LX, WB, ZhiZ and SZ performed the experiments. PF, LJ and JD analyzed and interpreted the data. FP, JL and DJ wrote the manuscript. ZhiZ and ZS supervised the study. FP and SZ confirm the authenticity of all the raw data. All authors read and approved the final version of the manuscript and agreed to be accountable for all aspects of the research in ensuring that the accuracy or integrity of any part of the work are appropriately investigated and resolved.

Ethics approval and consent to participate

The procedures involving animals were approved (approval no. S2019009) by the Ethics Committee for Laboratory Animals of Huazhong University of Science and Technology (Wuhan, China).

Patient consent for publication

Not applicable.

Competing interests

The authors declare that they have no competing interests.

References

1. Ritter J and Bielack SS: Osteosarcoma. Ann Oncol 21 (Suppl 7): vii320-vii325, 2010.
2. Isakoff MS, Bielack SS, Meltzer P and Gorlick R: Osteosarcoma: Current treatment and a collaborative pathway to success. J Clin Oncol 33: 3029-3035, 2015.
3. Bishop MW, Janeway KA and Gorlick R: Future directions in the treatment of osteosarcoma. Curr Opin Pediatr 28: 26-33, 2016.
4. Jarroux J, Morillon A and Pinskaya M: History, discovery, and classification of lncRNAs. Adv Exp Med Biol 1008: 1-46, 2017.
5. Zhu J, Fu H, Wu Y and Zheng X: Function of lncRNAs and approaches to lncRNA-protein interactions. Sci China Life Sci 56: 876-885, 2013.
6. Pu FF, Shi DY, Chen T, Liu YX, Zhong BL, Zhang ZC, Liu WJ, Wu Q, Wang BC, Shao ZW, *et al*: SP1-induced long non-coding RNA SNHG6 facilitates the carcinogenesis of chondrosarcoma through inhibiting KLF6 by recruiting EZH2. Cell Death Dis 12: 59, 2021.
7. Shi D, Wu F, Mu S, Hu B, Zhong B, Gao F, Qing X, Liu J, Zhang Z and Shao Z: LncRNA AFAP1-AS1 promotes tumorigenesis and epithelial-mesenchymal transition of osteosarcoma through RhoC/ROCK1/p38MAPK/Twist1 signaling pathway. J Exp Clin Cancer Res 38: 375, 2019.
8. Vaupel P, Schmidberger H, Mayer A. The Warburg effect: essential part of metabolic reprogramming and central contributor to cancer progression. Int J Radiat Biol 95: 912-919, 2019.
9. Dayton TL, Jacks T and Vander Heiden MG: PKM2, cancer metabolism, and the road ahead. EMBO Rep 17: 1721-1730, 2016.
10. Li YH, Li XF, Liu JT, Wang H, Fan LL, Li J and Sun GP: PKM2, a potential target for regulating cancer. Gene 668: 48-53, 2018.
11. Wong N, Ojo D, Yan J and Tang D: PKM2 contributes to cancer metabolism. Cancer Lett 356: 184-191, 2015.
12. Zhu S, Guo Y, Zhang X, Liu H, Yin M, Chen X and Peng C: Pyruvate kinase M2 (PKM2) in cancer and cancer therapeutics. Cancer Lett 503: 240-248, 2021.
13. Liu ZX, Hong L, Fang SQ, Tan GH, Huang PG, Zeng Z, Xia X and Wang XX: Overexpression of pyruvate kinase M2 predicts a poor prognosis for patients with osteosarcoma. Tumour Biol 37: 14923-14928, 2016.
14. Shang D, Wu J, Guo L, Xu Y, Liu L and Lu J: Metformin increases sensitivity of osteosarcoma stem cells to cisplatin by inhibiting expression of PKM2. Int J Oncol 50: 1848-1856, 2017.
15. Yuan Q, Yu H, Chen J, Song X and Sun L: Antitumor effect of miR-1294/Pyruvate Kinase M2 signaling cascade in osteosarcoma cells. Onco Targets Ther 13: 1637-1647, 2020.
16. Corley M, Burns MC and Yeo GW: How RNA-binding proteins interact with RNA: Molecules and mechanisms. Mol Cell 78: 9-29, 2020.
17. Bielli P and Sette C: Analysis of in vivo Interaction between RNA binding proteins and their RNA targets by UV cross-linking and immunoprecipitation (CLIP) method. Bio Protoc 7: e2274, 2017.
18. Chen T, Li Y, Cao W and Liu Y: miR-491-5p inhibits osteosarcoma cell proliferation by targeting PKM2. Oncol Lett 16: 6472-6478, 2018.
19. Chen X, Chen S and Yu D: Protein kinase function of pyruvate kinase M2 and cancer. Cancer Cell Int 20: 523, 2020.
20. Wyatt CA, Geoghegan JC and Brinckerhoff CE: Short hairpin RNA-mediated inhibition of matrix metalloproteinase-1 in MDA-231 cells: Effects on matrix destruction and tumor growth. Cancer Res 65: 11101-11108, 2005.
21. Livak KJ and Schmittgen TD: Analysis of relative gene expression data using real-time quantitative PCR and the 2(-Delta Delta C(T)) method. Methods 25: 402-408, 2001.
22. Xia H, Chen D, Wu Q, Wu G, Zhou Y, Zhang Y and Zhang L: CELF1 preferentially binds to exon-intron boundary and regulates alternative splicing in HeLa cells. Biochim. Biophys Acta Gene Regul Mech 1860: 911-921, 2017.

23. Xie C, Mao X, Huang J, Ding Y, Wu J, Dong S, Kong L, Gao G, Li CY and Wei L: KOBAS 2.0: A web server for annotation and identification of enriched pathways and diseases. Nucleic Acids Res 39: W316-W322, 2011.
24. Tang J, Yan T, Bao Y, Shen C, Yu C, Zhu X, Tian X, Guo F, Liang Q, Liu Q, *et al*: LncRNA GLCC1 promotes colorectal carcinogenesis and glucose metabolism by stabilizing c-Myc. Nat Commun 10: 3499, 2019.
25. Zhao Y, Liu Y, Lin L, Huang Q, He W, Zhang S, Dong S, Wen Z, Rao J, Liao W and Shi M: The lncRNA MACC1-AS1 promotes gastric cancer cell metabolic plasticity via AMPK/Lin28 mediated mRNA stability of MACC1. Mol Cancer 17: 69, 2018.
26. He L, Zhang H and Zhou X: Weanling offspring of dams maintained on serine-deficient diet are vulnerable to oxidative stress. Oxid Med Cell Longev 2018: 8026496, 2018.
27. Soga T, Baran R, Suematsu M, Ueno Y, Ikeda S, Sakurakawa T, Kakazu Y, Ishikawa T, Robert M, Nishioka T and Tomita M: Differential metabolomics reveals ophthalmic acid as an oxidative stress biomarker indicating hepatic glutathione consumption. J Biol Chem 281: 16768-16776, 2006.
28. Jin C, Zhu X, Wu H, Wang Y and Hu X: Perturbation of phosphoglycerate kinase 1 (PGK1) only marginally affects glycolysis in cancer cells. J Biol Chem 295: 6425-6446, 2020.
29. Liang Y, Song X, Li Y, Chen B, Zhao W, Wang L, Zhang H, Liu Y, Han D, Zhang N, *et al*: LncRNA BCRT1 promotes breast cancer progression by targeting miR-1303/PTBP3 axis. Mol Cancer 19: 85, 2020.
30. Yang XF, Zhou SY, Wang C, Huang W, Li N, He F and Li FR: Inhibition of LSD1 promotes the differentiation of human induced pluripotent stem cells into insulin-producing cells. Stem Cell Res Ther 11: 185, 2020.
31. Geng F, Cheng X, Wu X, Yoo JY, Cheng C, Guo JY, Mo X, Ru P, Hurwitz B, Kim SH, *et al*: Inhibition of SOAT1 suppresses glioblastoma growth via blocking SREBP-1-mediated lipogenesis. Clin Cancer Res 22: 5337-5348, 2016.
32. Loregger A, Raaben M, Nieuwenhuis J, Tan JM, Jae LT, van Den Hengel LG, Hendrix S, van Den Berg M, Scheij S, Song JY, *et al*: Haploid genetic screens identify SPRING/C12ORF49 as a determinant of SREBP signaling and cholesterol metabolism. Nat Commun 11: 1128, 2020.
33. World Medical Association and American Physiological Society: Guiding principles for research involving animals and human beings. Am J Physiol Regul Integr Comp Physiol 283: R281-R283, 2002.
34. Pu F, Chen F, Zhang Z, Qing X, Lin H, Zhao L, Xia P and Shao Z: TIM-3 expression and its association with overall survival in primary osteosarcoma. Oncol Lett 18: 5294-5300, 2019.
35. Tang T, Guo C, Xia T, Zhang R, Zen K, Pan Y and Jin L: LncCCAT1 promotes breast cancer stem cell function through activating WNT/β-catenin signaling. Theranostics 9: 7384-7402, 2019.
36. Yang W, Zheng Y, Xia Y, Ji H, Chen X, Guo F, Lyssiotis CA, Aldape K, Cantley LC and Lu Z: ERK1/2-dependent phosphorylation and nuclear translocation of PKM2 promotes the warburg effect. Nat Cell Biol 14: 1295-1304, 2012.
37. Iansante V, Choy PM, Fung SW, Liu Y, Chai JG, Dyson J, Del Rio A, D'Santos C, Williams R, Chokshi S, *et al*: PARP14 promotes the warburg effect in hepatocellular carcinoma by inhibiting JNK1-dependent PKM2 phosphorylation and activation. Nat Commun 6: 7882, 2015.
38. Liang J, Cao R, Zhang Y, Xia Y, Zheng Y, Li X, Wang L, Yang W and Lu Z: PKM2 dephosphorylation by Cdc25A promotes the warburg effect and tumorigenesis. Nat Commun 7: 12431, 2016.
39. Herjan T, Hong L, Bubenik J, Bulek K, Qian W, Liu C, Li X, Chen X, Yang H, Ouyang S, *et al*: IL-17-receptor-associated adaptor Act1 directly stabilizes mRNAs to mediate IL-17 inflammatory signaling. Nat Immunol 19: 354-365, 2018.
40. Abedini P, Fattahi A, Agah S, Talebi A, Beygi AH, Amini SM, Mirzaei A and Akbari A: Expression analysis of circulating plasma long noncoding RNAs in colorectal cancer: The relevance of lncRNAs ATB and CCAT1 as potential clinical hallmarks. J Cell Physiol 234: 22028-22033, 2019.
41. Yang W, Xia Y, Ji H, Zheng Y, Liang J, Huang W, Gao X, Aldape K and Lu Z: Nuclear PKM2 regulates β-catenin transactivation upon EGFR activation. Nature 480: 118-122, 2011.
42. Zhu H, Luo H, Zhu X, Hu X, Zheng L and Zhu X: Pyruvate kinase M2 (PKM2) expression correlates with prognosis in solid cancers: A meta-analysis. Oncotarget 8: 1628-1640, 2017.
43. Wiese EK and Hitosugi T: Tyrosine kinase signaling in cancer metabolism: PKM2 paradox in the warburg effect. Front Cell Dev Biol 6: 79, 2018.
44. Alquraishi M, Puckett DL, Alani DS, Humidat AS, Frankel VD, Donohoe DR, Whelan J and Bettaieb A: Pyruvate kinase M2: A simple molecule with complex functions. Free Radic Biol Med 143: 176-192, 2019.
45. Israelsen WJ and Vander Heiden MG: Pyruvate kinase: Function, regulation and role in cancer. Semin Cell Dev Biol 43: 43-51, 2015.
46. Luo W and Semenza GL: Emerging roles of PKM2 in cell metabolism and cancer progression. Trends Endocrinol Metab 23: 560-566, 2012.
47. Hombach S and Kretz M: Non-coding RNAs: Classification, biology and functioning. Adv Exp Med Biol 937: 3-17, 2016.
48. Li Q, Uemura Y and Kawahara Y: Cross-linking and immunoprecipitation of nuclear RNA-binding proteins. Methods Mol Biol 1262: 247-263, 2015.
49. Chen F, Wang Q, Yu X, Yang N, Wang Y, Zeng Y, Zheng Z, Zhou F and Zhou Y: MCPIP1-mediated NFIC alternative splicing inhibits proliferation of triple-negative breast cancer via cyclin D1-Rb-E2F1 axis. Cell Death Dis 12: 370, 2021.
50. Li W, Zhang Z, Liu X, Cheng X, Zhang Y, Han X, Zhang Y, Liu S, Yang J, Xu B, *et al*: The FOXN3-NEAT1-SIN3A repressor complex promotes progression of hormonally responsive breast cancer. J Clin Invest 127: 3421-3440, 2017.
51. Bhan A, Soleimani M and Mandal SS: Long noncoding RNA and cancer: A new paradigm. Cancer Res 77: 3965-3981, 2017.
52. Peng WX, Koirala P and Mo YY: LncRNA-mediated regulation of cell signaling in cancer. Oncogene 36: 5661-5667, 2017.
53. Sanchez Calle A, Kawamura Y, Yamamoto Y, Takeshita F and Ochiya T: Emerging roles of long non-coding RNA in cancer. Cancer Sci 109: 2093-2100, 2018.
54. Tao T, Wu S, Sun Z, Ma W, Zhou S, Deng J, Su Q, Peng M, Xu G and Yang X: The molecular mechanisms of LncRNA-correlated PKM2 in cancer metabolism. Biosci Rep 39: BSR20192453, 2019.
55. Puckett DL, Alquraishi M, Chowanadisai W and Bettaieb A: The role of PKM2 in metabolic reprogramming: Insights into the regulatory roles of non-coding RNAs. Int J Mol Sci 22: 1171, 2021.
56. Wang C, Li Y, Yan S, Wang H, Shao X, Xiao M, Yang B, Qin G, Kong R, Chen R and Zhang N: Interactome analysis reveals that lncRNA HULC promotes aerobic glycolysis through LDHA and PKM2. Nat Commun 11: 3162, 2020.
57. Panasyuk G, Espeillac C, Chauvin C, Pradelli LA, Horie Y, Suzuki A, Annicotte JS, Fajas L, Foretz M, Verdeguer F, *et al*: PPAR gamma contributes to PKM2 and HK2 expression in fatty liver. Nat Commun 3: 672, 2012.
58. Zhao X, Zhao L, Yang H, Li J, Min X, Yang F, Liu J and Huang G: Pyruvate kinase M2 interacts with nuclear sterol regulatory element-binding protein 1a and thereby activates lipogenesis and cell proliferation in hepatocellular carcinoma. J Biol Chem 293: 6623-6634, 2018.
59. Eberle D, Hegarty B, Bossard P, Ferré P and Foufelle F: SREBP transcription factors: Master regulators of lipid homeostasis. Biochimie 86: 839-848, 2004.
60. Horton JD, Goldstein JL and Brown MS: SREBPs: Activators of the complete program of cholesterol and fatty acid synthesis in the liver. J Clin Invest 109: 1125-1131, 2002.
61. Zeng L, Lu M, Mori K, Luo S, Lee AS, Zhu Y and Shyy JY: ATF6 modulates SREBP2-mediated lipogenesis. EMBO J 23: 950-958, 2004.

This work is licensed under a Creative Commons Attribution-NonCommercial-NoDerivatives 4.0 International (CC BY-NC-ND 4.0) License.